arXiv:astro-ph/0012150v1 6 Dec 2000

Deep HST Imaging of IC 1613. I. Variable Stars and Distance[1]

Andrew E. Dolphin, A. Saha

National Optical Astronomy Observatories, P.O. Box 26372, Tucson, AZ 85726

Electronic mail: dolphin@noao.edu, saha@noao.edu

Evan D. Skillman

Astronomy Department, University of Minnesota, Minneapolis, MN 55455

Electronic mail: skillman@astro.umn.edu

Eline Tolstoy

UK Gemini Support Group, Astrophysics, NAPL, University of Oxford, Keble Road,

Oxford OX1 3RH, UK

Electronic mail: etolstoy@astro.ox.ac.uk

A.A. Cole

Physics & Astronomy Dept., 538 LGRT, University of Massachusetts, Amherst, MA 01003

Electronic mail: cole@condor.astro.umass.edu

R.C. Dohm-Palmer

University of Michigan, Dept. of Astronomy, 821 Dennison Building, Ann Arbor, MI

48109-1090

Electronic mail: rdpalmer@astro.lsa.umich.edu

J.S. Gallagher

[1] Based on observations with the NASA/ESA *Hubble Space Telescope*, obtained at the Space Telescope Science Institute, which is operated by the Association of Universities for Research in Astronomy, Inc., under NASA contract NAS 5-26555. These observations are associated with proposal ID 7496.

University of Wisconsin, Dept. of Astronomy, 475 N. Charter St, Madison, WI 53706

Electronic mail: jsg@astro.wisc.edu

Mario Mateo

University of Michigan, Dept. of Astronomy, 821 Dennison Building, Ann Arbor, MI 48109-1090

Electronic mail: mateo@astro.lsa.umich.edu

J.G. Hoessel

University of Wisconsin, Dept. of Astronomy, 475 N. Charter St, Madison, WI 53706

Electronic mail: hoessel@astro.wisc.edu

Received _____; accepted _____

ABSTRACT

We present WFPC2 VI photometry of a field in the halo of IC 1613, finding 13 RR Lyraes and 11 Cepheids. Our photometry of the red giant branch tip and red clump is used to derive distances to IC 1613, which are consistent with each other and with distances based on the variable stars. We compare these values with similarly-measured distances for the Magellanic Clouds, and are able to measure metallicity dependencies of the RR Lyrae and Cepheid distances by requiring consistent relative distance measurements from the four techniques. For metallicities of [Fe/H] $= -1.3$ (RR Lyraes) and -1.0 (Cepheids), we find a relatively steep slope of 0.34 ± 0.20 magnitudes per dex for the RR Lyraes and a shallow slope of -0.07 ± 0.16 mag/dex for the Cepheids, both values within the range of theoretical and empirical results in the literature. We find that a dependence of the red clump absolute magnitude on age, in addition to metallicity, is required to produce self-consistent relative distances between IC 1613 and the Magellanic Clouds. Adopting such a red clump calibration and self-consistent calibrations for the other three distance indicators, we find that the distances to all three objects are in excellent agreement. Our best distance modulus to IC 1613 is $\mu_0 = 24.31 \pm 0.06$, corresponding to a distance of 730 ± 20 kpc. This distance produces an RR Lyrae absolute magnitude of $M_V = 0.61 \pm 0.08$.

Subject headings: Cepheids — galaxies: distances and redshifts — galaxies: individual (IC 1613) — Local Group — stars:variables:other

1. Introduction

Studies of the stellar populations in nearby galaxies provide a powerful tool for determining the key physical parameters of galaxy evolution such as the age (star formation history), the chemical composition and enrichment history, the stellar initial mass function, environmental effects, and the dynamical history of the system. Using the HST, it is possible to photometer individual stars down to very faint magnitudes, and to interpret the observable parameters such as the morphology of the color-magnitude diagram (CMD). This approach is a logical stepping stone to understanding galaxy evolution and provides a physical basis for understanding observations of high redshift galaxies and their implications for cosmological models. Detailed analysis of the intermediate and old stellar populations of Local Group galaxies should reveal histories in accordances with those implied by studies of galaxies at higher redshift (Tolstoy 1999). With the appropriate data, which currently are obtained primarily by using HST, this hypothesis can be directly tested.

Here we are presenting new HST observations of a field in the halo of IC 1613, a dwarf irregular galaxy in the Local Group. In this paper we concentrate on the variable stars of IC 1613 and, in particular, their relevance to its distance determination. In a future paper, we will reconstruct the star formation history of IC 1613 by analysis of the stellar populations.

The known properties of IC 1613 have recently been summarized by van den Bergh (2000). We will give only a short summary of relevant properties. Because of its proximity (distance ~ 720 kpc), its high galactic latitude (-60.6^o) and thus little galactic extinction, and its inclination (38^o, Lake & Skillman 1989), IC 1613 provides an excellent opportunity to observe stellar populations in a relatively low-metallicity environment. Interestingly, there are few studies of the metallicity in IC 1613. Mateo (1998) gives a value of the mean iron abundance for the old and intermediate age stellar populations of [Fe/H] $= -1.3 \pm 0.2$ (from Lee et al. 1993 using the RGB color at $M_I = -3.5$; see also Cole et al. 1999) and an

oxygen abundance of the interstellar medium of $12 + \log(\mathrm{O/H}) = 7.8 \pm 0.2$ (Talent 1980). Due to the high Galactic latitude, the reddening to IC 1613 is very low, and here we adopt an extinction of $A_V = 0.08 \pm 0.02$ from Schlegel et al. (1998).

The distance to IC 1613 was determined from Cepheid variable stars early on by Baade (Sandage 1971) and, based in part on the observations of Cepheids by Freedman (1988), Madore & Freedman (1991) placed IC 1613 at a distance of 765 kpc ($\mu_0 = 24.42 \pm 0.13$). Saha et al. (1992) observed RR Lyrae variable stars and derived a distance of 660 kpc ($\mu_0 = 24.10 \pm 0.27$). Using the observation of the tip of the red giant branch, Lee et al. (1993) derived a distance of 714 kpc ($\mu_0 = 24.27 \pm 0.25$), a value confirmed by the WFPC2 study of an inner field of IC 1613 by Cole et al. (1999). These values are all consistent within the errors, but their differences may be dominated by systematic errors.

Cole et al. (1999) presented an initial study of IC 1613 stellar populations, based on 10700s of integration in both F555W and F814W, as well as 2600s in F439W, of a field nearer the center of the galaxy. They found evidence of a continuous star forming history, with the presence of all expected components of the CMD (main sequence, red supergiants, blue and red helium burners, asymptotic red giants, red giants, and a red clump), as well as a hint of a blue horizontal branch. From the CMD morphology of the central field, Cole et al. derived an approximate age-metallicity relation for IC 1613, finding it similar in form to that of the SMC but ~ 0.3 dex more metal-poor at any given age. Their data were not designed for variable star study (the primary goal of this paper), however, so we will leave a detailed comparison between their results and those from these data for a future paper on the stellar populations.

A critical issue in the use of extragalactic stellar distance indicators is their sensitivity to changes in metallicity. This question received a good deal of attention in the recent literature (e.g., Kennicutt et al. 1998, Sandage, Bell, & Tripicco 1999, Caputo, and

Marconi, & Musella 2000 for discussions of the Cepheid scale; McNamara 1997, Caputo et al. 2000, and Demarque et al. 2000 for RR Lyraes; Lee et al. 1993 and Salaris & Cassisi 1998 for the RGB tip; and Girardi & Salaris 2000 and Udalski 2000 for the red clump). A fundamental point in these discussions is whether offsets due to metallicity are more or less important than uncertainties in the various luminosity zero points. Since the first rung of the variable star distance ladder is the Magellanic Clouds, which are moderately metal-poor, observations of similar galaxies, such as IC 1613, provide the opportunity to empirically test for the importance of modest variations in metallicity among metal-poor systems. In the present observations, we are able to measure the magnitudes of four independent "standard candles" – RR Lyrae variable stars, Cepheid variable stars, the tip of the red giant branch, and the mean magnitude of the red clump – in a galaxy that has slightly lower metallicity than the Small Magellanic Cloud. By comparing these four distance determinations to those of the Magellanic Clouds, we are able to test for systematic differences associated with each indicator and potential metallicity dependencies.

2. Data and Reduction

2.1. Observations

WFPC2 observations of a field in the halo of IC 1613 were obtained during 22-27 August 1999, as part of program GO-7496, whose purpose is to investigate the stellar populations of dwarf irregular galaxies. The field center (01^h 04^m 26.7^s, +02° 03' 16", J2000) is located 11.6' southwest of the center of the galaxy and 6.7' southwest of the field studied by Cole et al. (1999). There is no overlap with the field examined by Saha et al. (1992) in the previous IC 1613 RR Lyrae study, which is 14.6' to the west, or with the field of Antonello et al. (1999). The data consist of 48 1200s images: 16 in F555W and 32 in F814W, spread evenly among four dithering pointings. Each orbit consisted of two images

in the same filter to aid in cosmic ray removal. A 25th orbit was used to obtain two F656N (H_α) images, which were used for other purposes, but not for the variable star work that is the topic of this paper.

2.2. Reductions

The data were obtained from the STScI archive using on the fly calibration, and thus were pipeline-calibrated using the best available calibration images at the time of retrieval. The images were then reduced using the HSTphot package (Dolphin 2000a). The data quality image (c1f) was used to mask bad and questionable pixels, and the pairs of images from each orbit were combined for cosmic ray removal, producing 8 clean 2400s images in F555W and 16 images in F814W. A deep image produced from combining all eight F814W images at the first pointing is shown in Figure 1. The sky image (which contains calculated sky values at each pixel and is determined before running photometry for uncrowded images for greater efficiency) was then calculated and hot pixels removed using the HSTphot utilities.

EDITOR: PLACE FIGURE 1 HERE.

Photometry was made using the *multiphot* routine of HSTphot, which solves the photometry simultaneously on multiple images (all 24, in this case) in order to reduce the number of free parameters. The detection threshold was a minimum signal to noise of 3.5 in both the combined F555W and combined F814W measurements. CTE loss corrections and calibrations were made using Dolphin (2000b). Because of the presence of bright, isolated stars, PSF solutions and aperture corrections were made for each chip of each image. The color-magnitude diagram is shown in Figure 2, using all stars with the goodness-of-fit parameter $\chi \leq 1.5$, |object sharpness| ≤ 0.3 (sharpness of a perfect star is zero), and

total signal-to-noise of at least 5 in both F555W and F814W. In order to eliminate poor detections, these requirements were also made on the detections at each epoch, with detections failing to meet the χ, sharpness, and signal-to-noise criteria eliminated. To verify the accuracy of our photometry, we reduced the data at one pointing independently, using DoPHOT procedures described by Saha et al. (1996). This comparison is shown in detail in Dolphin (2000a), with agreement to within 0.01 magnitudes in both filters.

EDITOR: PLACE FIGURE 2 HERE.

Before proceeding with the variable star search, it was necessary to determine the maximum accuracy of the photometry. This was done by comparing the magnitudes of well-measured upper red giant branch stars at each epoch with the combined magnitudes. This comparison, which tests both the reliability of the photometry and that of the aperture corrections, showed a median scatter of 0.015 magnitudes. This value was adopted as the minimum error in the variable star work, with all smaller photometric uncertainties increased to 0.015 magnitudes. The source of this error is a combination of photometric error from the undersampled images and error in the aperture corrections.

Figure 3 shows the scatter (individual epoch minus combined magnitude) for all stars. The locations of the Cepheids (F555W of $\sim 22 - 23$) and RR Lyraes (F555W of ~ 25) are shown by the excess scatter, and the limiting accuracy of 0.015 magnitudes at the bright end is clear. Otherwise, the figure is typical for a star-forming dwarf.

EDITOR: PLACE FIGURE 3 HERE.

2.3. Variable Star Identification

Variable star candidates were identified using a procedure similar to that described by Saha & Hoessel (1990). For a star to be considered a candidate variable, it had to meet four criteria. First, the star had to have good photometry in at least 16 of the 24 epochs, and an rms scatter of at least 0.08 magnitudes. Second, the reduced χ^2 of the photometry, as defined by

$$\chi^2 = \frac{1}{N_{F555W} + N_{F814W}}\left(\sum_{i=1}^{N_{F555W}} \frac{(F555W_i - \overline{F555W})^2}{\sigma_i^2} + \sum_{i=1}^{N_{F814W}} \frac{(F814W_i - \overline{F814W})^2}{\sigma_i^2}\right), \quad (1)$$

had to be at least 6.25, where N_{F555W} and N_{F814W} are the numbers of exposures in the two filters, and $F555W_i$ and $F814W_i$ are the magnitudes at each epoch, and $\overline{F555W}$ and $\overline{F814W}$ are the mean magnitudes for each star. The minimum value of 6.25 corresponds to mean deviation of 2.5σ, and was determined empirically for these data. A second χ^2 test was made in order to reduce the ability of single bad points to cause a false detection. The one-third of the points contributing the most to χ^2 were eliminated, and the reduced χ^2 recalculated from the remaining points. If this value was not at least 0.25, the star was eliminated from the list of candidate variables. Again, the value of 0.25 was determined empirically.

Finally, a modified Lafler-Kinman algorithm (Lafler & Kinman 1965) was used to test the stars for periodicity. This was implemented by computing Θ for periods between 0.1 and 5.0 days. The Θ parameter is calculated by determining the light curve for a trial period and using the equation

$$\Theta(p) = \frac{\sum_{i=1}^{N}(m_i - m_{i+1})^2}{\sum_{i=1}^{N}(m_i - \overline{m})^2}, \quad (2)$$

where N is the number of exposures for a given filter, m_i is the magnitude at epoch i, and $\overline{m}$ is the mean magnitude. If the trial period is incorrect, $m_i - m_{i+1}$ will be the difference between two random points, $\sqrt{2}$ times the rms scatter, producing a Θ of 2. However, if the

trial period is correct, the difference between adjacent points will scale as $1/N$, producing a Θ that scales as $1/N^2$. A goodness of periodicity parameter can then be defined as $\Lambda(p) = 2/\Theta(p)$. For this study, the off-period Θ was defined to be the 90th percentile value of Θ over the range of trial periods, giving our goodness of periodicity parameter of $\Lambda(p) = \Theta_{90}/\Theta(p)$.

For the present data set, however, a sufficient number of observations was made in both F555W and F814W for light curve measurements to be made in both filters. Thus a combined goodness of periodicity parameter needed to be developed. Given that $\sqrt{\Lambda}$ scales as the number of observations in a given filter when at the correct period, a reasonable combined parameter would be

$$\Lambda = 0.25(\sqrt{\Lambda_{F555W}} + \sqrt{\Lambda_{F814W}})^2, \tag{3}$$

where the constant of 0.25 is included to force the off-period Λ to 1. In the general case, a goodness of periodicity for any number of filters can be calculated with

$$\Lambda = (\frac{1}{N_{filt}} \sum_{i=1}^{N_{filt}} \sqrt{\Lambda_i})^2. \tag{4}$$

For this study, Λ was required to be at least 2.0 for a star to be considered a candidate variable.

We note that, because Θ is statistically independent of amplitude (doubling the amplitude would leave Θ unchanged, for example), our determination of Λ does not account for the larger amplitudes of RR Lyraes and Cepheids in $F555W$. It is not immediately obvious if or how such an accounting should be made. Nevertheless, we have experimented with other algorithms for the calculation of Λ and Θ, such as

$$\Theta(p) = \frac{\sum_{i=1}^{N_{F555W}} (F555W_i - F555W_{i+1})^2 + \sum_{i=1}^{N_{F814W}} (F814W_i - F814W_{i+1})^2}{\sum_{i=1}^{N_{F555W}} (F555W_i - \overline{F555W})^2 + \sum_{i=1}^{N_{F814W}} (F814W_i - \overline{F814W})^2}, \tag{5}$$

and find the selection of variables and their periods to be quite robust, regardless of the choice of algorithm.

Out of the 12983 total stars, the steps listed above selected 57 variable star candidates, which were examined interactively. As this study is primarily concerned with pulsating variables, stars that were variable in only one filter and stars whose F555W and F814W light curves were out of phase were removed from the candidate list, as were false detections, leaving 26 stars in the list. Eleven fall in the instability strip above the horizontal branch, and were classified as Cepheids. Thirteen fall along the horizontal branch, and were classified as RR Lyraes. The remaining two are possible eclipsing binaries. Figure 4 shows the IC 1613 CMD, with the variable stars highlighted. It should be emphasized that our detection efficiency was not 100% (and was much lower for stars with period greater than 0.6 days, the duration of our longest set of consecutive orbits). Thus we cannot rule out the existence of Population II Cepheids, nor are we confident that the "non-variable" stars falling within the instability strip are not, in fact, variables that were not detected. Additionally, while the CMD from combined photometry is largely complete to $I = 27$, the single epoch signal-to-noise of stars below the horizontal branch is such that detection of variables would have been extremely difficult.

EDITOR: PLACE FIGURE 4 HERE.

Mean magnitudes were calculated for each variable, using a period-weighted average

$$\langle m \rangle = -2.5 \log \sum_{i=1}^{N} \frac{\phi_{i+1} - \phi_{i-1}}{2} 10^{-0.4 m_i}, \tag{6}$$

where ϕ_i is the phase and m_i is the magnitude at each point along the light curve. These values, still in WFPC2 F555W and F814W magnitudes, were then transformed to standard V and I.

3. Analysis

3.1. RR Lyraes

Figure 5 shows the light curves of the thirteen RR Lyrae candidates, and Table 1 contains their positions and data. All positions are given relative to the F555W images at the first pointing. The final column in Table 1 lists the quality of the light curve, from 0 to 4 (although all stars with quality values of 0 or 1 have been removed). The criteria that are used to determine the light curve quality are the uniqueness of the period, the presence or lack of bad points, light curves in phase between the two filters, and the resemblance to a template light curve of the appropriate class of object. We do not attempt to distinguish between fundamental-mode and overtone pulsators in the RR Lyraes, given the relatively poor signal-to-noise at each epoch (the typical uncertainty in both filters is 0.1 magnitudes). However, we do note that the short periods of variables V14 and V16 make them likely overtone pulsators, and that those of V19 and V23 make them possible overtone pulsators.

EDITOR: PLACE FIGURE 5 HERE.

EDITOR: PLACE TABLE 1 HERE.

Multiplying the uncertainties in $\langle V \rangle$ by 4 divided by the light curve quality, and taking an average weighted by $1/\sigma^2$, the best $\langle V \rangle$ for the sample of 13 RR Lyraes is 25.00 ± 0.03 magnitudes. Eliminating the two possible outliers fainter than V=25.2, the weighted average is 24.98 ± 0.03. Similarly eliminating the two possible outliers brighter than V=24.8, the weighted average becomes 25.02 ± 0.03. Given the very small shift in the mean magnitude after eliminating the lowest and highest points, it seems reasonable to adopt the value of $\langle V \rangle = 25.00$ for the mean RR Lyrae magnitude, while adding the ± 0.02 shift in quadrature to the 0.03 magnitude uncertainty, producing a final uncertainty of 0.04 magnitudes. This mean V magnitude is consistent with the value of $\langle g \rangle = 24.90 \pm 0.10$

obtained by Saha et al. (1992), which corresponds to a mean V magnitude of 24.94 ± 0.10 (Saha & Hoessel 1987). An extinction A_V of 0.08 magnitudes is adopted from Schlegel et al. (1998) (assuming $A_V/A_B = 3.1/4.1$), with the uncertainty estimated to be ± 0.02 magnitudes, producing an extinction-corrected mean V magnitude of $\langle V \rangle_0 = 24.92 \pm 0.04$.

Once the mean V magnitude is established, obtaining a distance estimate requires a value for the absolute magnitude. This is generally done by adopting a value for the mean RR Lyrae metallicity and a preferred M_V vs. [Fe/H] relation. We can measure the mean RR Lyrae metallicity via the red giant branch, whose tip spans the color range $1.45 < (V - I) < 1.62$. Assuming that RR Lyraes are only produced in populations older than 10 Gyr, we find an allowable metallicity range of $-1.5 <$ [Fe/H] < -1.1 (with [Fe/H] $= -1.5$ and $t = 15$ Gyr falling along the blue edge of our RGB and [Fe/H] $= -1.1$ and $t = 10$ Gyr falling along the red edge), based on isochrones interpolated from those of Girardi et al. (2000). Thus we find a value of [Fe/H] $= -1.3 \pm 0.2$ for the RR Lyrae metallicity. For comparison, metallicity calculations using the Da Costa & Armandroff (1990) $(V - I)_{M_I=-3.0}$ and Lee et al. (1993) $(V - I)_{M_I=-3.5}$ calibration produce the identical metallicity ([Fe/H] $= -1.3 \pm 0.2$), after conversion to the Carretta & Gratton (1997) metallicity scale.

The range of resulting absolute magnitudes is rather large, however, producing significant uncertainty in the RR Lyrae distance. Theoretical models of Girardi et al. (2000) predict an absolute magnitude of $M_V = 0.60 \pm 0.03$; those of Demarque et al. (2000) produce an absolute magnitude of $M_V = 0.62 \pm 0.05$; and those of Caputo et al. (2000) produce an absolute magnitude of $M_V = 0.57 \pm 0.12$. Carretta et al. (2000) find a relation based on LMC distances and HIPPARCOS parallax measurements of subdwarfs that produces an absolute magnitude of $M_V = 0.59 \pm 0.07$. Other theoretical models produce brighter RR Lyraes, with Caloi et al. (1997) and Cassisi et al. (1999) finding $M_V \approx 0.55$

for the ZAHB; the mean RR Lyrae magnitude being about 0.1 magnitudes brighter. Observational determinations based on HIPPARCOS show a larger spread in values, such as those of Fernley et al. 1998, which produces an absolute magnitude of $Mv = 0.73 \pm 0.14$, and Gratton et al. 1997, which produces an absolute magnitude of $Mv = 0.45 \pm 0.04$. We therefore conservatively adopt a value of $M_V = 0.60 \pm 0.15$, which produces an distance modulus of 24.32 ± 0.16. We will return to the issue of the RR Lyrae zero point later, using independent distance measurements to derive the absolute magnitude of RR Lyraes in IC 1613.

3.2. Cepheids

Although the observations were designed primarily to detect RR Lyraes, eleven short-period Cepheids were also discovered. Figure 6 shows their light curves, and Table 2 contains their positions and data. As with Table 1, the quality rating ranges from 0 to 4, with 4 being the cleanest light curve and best-defined period. The Cepheids were also classified into fundamental-mode and overtone pulsators, with all but V13 classified based on their light curves. As shown by Mantegazza & Poretti (1992), overtone pulsators have a Fourier spectrum with a weaker second order than do fundamental pulsators, meaning that their light curves will be more sinusoidal. Ten of the eleven Cepheids were thus classified, and the period-luminosity relation in Figure 7 shows this discrimination to be successful, with all overtone pulsators falling well above the mean period-luminosity relation. The period of V13 was poorly-constrained due to the poor sampling of epochs, and thus it could not be classified similarly. However, its position on the period-luminosity relation was clearly in the space occupied by overtone pulsators, allowing its classification based on period and magnitude.

EDITOR: PLACE FIGURE 6 HERE.

EDITOR: PLACE TABLE 2 HERE.

The presence of five fundamental-mode Cepheids allows for a second distance measurement from these data. One can do this following Madore & Freedman (1991), determining the reddening-free magnitude $W = 2.43I - 1.43V$ (assuming $A_V/A_I = 1.7$) for the five Cepheids and calculate the reddening-free absolute magnitude $M_W = -3.049 \log P - 2.40$ using the Madore & Freedman (1991) calibration. Applying this technique to the IC 1613 fundamental Cepheids and using a weighted average of the uncertainties gives a reddening-corrected distance modulus of $\mu_0 = 24.50 \pm 0.11$ and a mean extinction A_V of 0.16 ± 0.11 magnitudes. The V and I period-luminosity relations are shown in Figure 7, with the Cepheids found by Freedman (1988) plotted as well. As can be seen in the Figure, the present data are consistent with and provide an extension to the longer-period data of Freedman (1988).

EDITOR: PLACE FIGURE 7 HERE.

However, the EROS result (Bauer et al. 1999) of a steepening in the period-luminosity relation for periods shorter than two days implies that three of our five fundamental-mode Cepheids should be eliminated from this calculation. (This break is shown with the dashed line in Figure 7.) Thus the reddening-corrected distance modulus becomes $\mu_0 = 24.55 \pm 0.18$ for the two remaining fundamental-mode Cepheids. The large uncertainty is the result of the use of the reddening-free distance, which multiplies V uncertainties by 2.43 and I by 1.43 and adds them in quadrature. Given the low extinction to IC 1613 and the presence of a good extinction estimate of $A_V = 0.08 \pm 0.02$, the uncertainty can be lowered by correcting the individual V and I distance moduli for extinction and combining them.

Finally, it should be noted that the I photometry of V3 do not adequately sample the full range of the light curve, as the earliest epoch was at a phase of 0.2 after the peak.

Thus the phase-averaged $\langle I \rangle$ magnitude is biased towards fainter magnitudes. Because this was not a problem in the V photometry, the procedure of Labhardt, Sandage, & Tammann (1997) was used to calculate the correct mean $\langle I \rangle$, brightening the value from 21.21 to 21.15. The data for V6 have a similar problem, but a similar correction is impossible because neither the V nor I photometry span the entire range of magnitudes. However, because the V light curve omits as much of the trough as the I light curve omits of the peak, these errors should largely cancel when averaging the V and I distances obtained for V6.

Table 3 shows the mean V and I magnitudes corrected for extinction values $A_V = 0.08 \pm 0.02$ and $A_I = 0.05 \pm 0.02$. Absolute magnitudes M_V and M_I are calculated using Madore & Freedman (1991), with their rms scatter adopted as the uncertainties. Given the smaller intrinsic scatter in the I period-luminosity relation, the distance for each of the Cepheids is weighted twice as much in I as in V. Averaging the values for the two stars gives a best Cepheid distance from these data of $\mu_0 = 24.45 \pm 0.15$ magnitudes, consistent with the value of $\mu_0 = 24.42 \pm 0.13$ determined by Madore & Freedman (1991) from the Cepheid calibration used here, as well as with previous measurements of Sandage (1971); McAlary, Madore, & Davis (1984); and Freedman (1988). The values in Figure 7 are for this distance and the adopted extinction, with the dashed line showing the expected V relation for $P < 2^d$ based on the EROS result. Because of their larger sample size, we will adopt the Madore & Freedman (1991) value in our discussion, after converting it to our adopted extinction of $A_V = 0.08$ for the sake of comparison with other distance measurements. This decreases their distance to $\mu_0 = 24.40 \pm 0.13$. We will discuss possible metallicity effects on the Cepheid distance scale below.

EDITOR: PLACE TABLE 3 HERE.

3.3. Other Distance Measurements

Although variable stars provide excellent distance indicators, there remain questions about the zero-point calibrations at the 20% level, as well as uncertainties regarding their dependencies on the metallicity of the parent population of stars. These issues will be discussed in the following section. IC 1613 provides us also with additional distance benchmarks, which provide further constraints for studying this problem.

The red giant branch (RGB) tip (Lee, Madore, & Freedman 1993) and red clump (Paczynski & Stanek 1998, Udalski 2000) provide two possible standard candles. The RGB tip in I is especially attractive, given its insensitivity to age and metallicity in theoretical models (Girardi et al. 2000, for example). From the CMD in Figure 2 and an edge-detection algorithm, we measure an RGB tip at $I = 20.40 \pm 0.09$. However, this value is something of an upper limit to the RGB tip magnitude, as the small number of stars present in the upper RGB makes it plausible that the theoretical RGB extends above the position of these stars. With an upper RGB luminosity function of roughly 7 stars per 0.1 magnitudes, our 68% confidence limit for the true RGB tip is 0.03 magnitudes above the brightest star, increasing our uncertainty in the RGB tip measurement to 0.10 magnitudes.

We can derive a more accurate RGB tip by use of the denser field studied by Cole et al. (1999), which contains significantly more red giants. Reducing those data with HSTphot and applying the Dolphin (2000b) CTE correction and calibration, we find the RGB tip at $I = 20.35 \pm 0.07$, consistent with that determined for the present data (the 0.07 magnitude uncertainty a result of possible RGB-AGB confusion near the tip). The luminosity function for the upper RGB is shown in Figure 8. Applying our adopted extinction correction of $A_I = 0.05 \pm 0.02$ produces an extinction-corrected RGB tip magnitude of $I_0 = 20.30 \pm 0.07$. We find the photometry of Cole et al. nearly 0.1 magnitudes brighter, and note that we adopt the HSTphot-based photometry for the inner field, as it is more consistent with the

photometry for the outer field (which was consistent with DoPHOT reductions of the same data), and because of the availability of an HSTphot-based calibration and CTE correction (Dolphin 2000b).

EDITOR: PLACE FIGURE 8 HERE.

The absolute magnitude at the RGB tip can be estimated either empirically (Lee et al. 1993) or theoretically (Girardi et al. 2000). Empirical calibrations rest on the globular cluster distance scale, which is itself dependent upon an assumed RR Lyrae absolute magnitude calibration, and thus cannot be used to make an *independent* distance measurement for our study. Theoretical techniques, on the other hand, are subject to uncertainties in the input physics (Castellani & degl'Innocenti 1999) and the transformation from physical parameters (luminosity and temperature) to observed magnitudes and colors. In order to produce an independent distance measurement and to account for the uncertainties, we thus adopt an absolute magnitude calculated from interpolated isochrones from Girardi et al. (2000), while conservatively adding the difference between this value and that calculated from the Lee et al. (1993) calibration to our uncertainties. Fitting the isochrones to our red giant branch for ages from 2 to 15 Gyr, we measure a mean metallicity of [Fe/H] $= -1.15 \pm 0.2$ and absolute magnitude of $M_I = -4.02 \pm 0.02$. For comparison, the calibration given by Lee et al. (1993), using the equivalent metallicity on the Zinn & West (1984) scale ([Fe/H] $= -1.37$ from the conversion given by Carretta & Gratton 1997), produces an absolute magnitude of $M_I = -4.06 \pm 0.04$, consistent but 0.04 magnitudes brighter. We thus arrive at an RGB tip absolute magnitude of $M_I = -4.02 \pm 0.05$ and a distance modulus of $\mu_0 = 24.32 \pm 0.09$.

We note that the RGB tip calibration of Salaris & Cassisi (1998) provides a significantly more luminous tip, at $M_I = -4.25 \pm 0.02$, which would increase the IC 1613 distance modulus to $\mu_0 = 24.55 \pm 0.07$. We are unable to reconcile this value with the red clump

distance (below), regardless of the star formation history assumed for IC 1613. Because the red clump is the only one of the four distance indicators calibrated directly by HIPPARCOS, we choose to adopt the calibration above of $M_I = -4.02 \pm 0.05$, with the RGB tip distance modulus of $\mu_0 = 24.32 \pm 0.09$.

Another independent measurement of the distance is provided by the mean I magnitude of the red clump. Although M_I(RC) varies significantly with both age and metallicity (for example, Girardi et al. 1998 and Girardi & Salaris 2000 for theoretical work; Sarajedini 1999 for empirical work), Girardi & Salaris (2000) have demonstrated that it can be adequately modeled, and used as an accurate distance indicator that provides distances consistent with other, more-tested, distance measurements.

The measurement of the red clump mean magnitude is relatively easy, aided by the separation of the two features in the CMD. Figure 9 shows the I luminosity function for stars with $0.8 \leq V - I \leq 0.95$ and $22 \leq I \leq 25.5$, with the best-fit polynomial (RGB) plus Gaussian (red clump) shown. The peak of the Gaussian falls at $I = 23.90 \pm 0.01$ (uncertainties derived using bootstrap tests and a variety of bin sizes), which corresponds to an extinction-corrected value of $I_0 = 23.85 \pm 0.02$. For comparison, our HSTphot-reduced photometry of the inner field (the field studied by Cole et al. 1999) produces a slightly brighter red clump magnitude of $I = 23.86 \pm 0.01$. The difference of 0.04 magnitudes is statistically significant; the most likely explanation is the presence of a larger fraction of young ($t \lesssim 1$ Gyr) stars in the inner field.

EDITOR: PLACE FIGURE 9 HERE.

Determination of the red clump absolute magnitude, however, is significantly more difficult. Udalski (2000) provides an empirical calibration of $M_I(RC)$ vs. metallicity, but this calibration would have to be extrapolated by nearly a dex in metallicity for application

to IC 1613 and is based on the assumption that there is no age-metallicity relation in the Galactic disk. Neither of those problems can be easily solved analytically, so we instead employ the Girardi et al. (2000) theoretical isochrones as an accurate relative absolute magnitude indicator, with which we can compare the local disk clump with that of IC 1613 (a method very similar to "method 2" of Girardi & Salaris 2000). We produced a synthetic CMD for the local Galactic disk based on the age-metallicity relation and star ages of Table 3 of Rocha-Pinto et al. (2000), and a set of 15 synthetic CMDs for IC 1613 based on a range of possible age-metallicity relations and star formation histories consistent with the results of Cole et al. (1999). Applying the usual Gaussian clump plus quadratic RGB fit to the synthetic CMDs, we measure a difference of $\delta M_I = -0.22 \pm 0.08$ magnitudes between the IC 1613 red clump and the Galactic disk red clump, in the sense that the IC 1613 clump is brighter. Combined with the HIPPARCOS-based local red clump calibration of $M_I = -0.23 \pm 0.02$ (Stanek & Garnavich 1998), we derive a semi-empirical IC 1613 red clump absolute magnitude of $M_I = -0.45 \pm 0.09$ and a red clump distance modulus of $\mu_0 = 24.30 \pm 0.09$.

Thus, two additional independent distances can be obtained by use of the RGB tip and the red clump. The RGB tip distance is corrected for age and metallicity relatively easily, but difficulty in observational determination of the tip magnitude and uncertainty in the calibration create additional error. In contrast, the red clump position is easily measured with high precision, but the systematics from age- and metallicity-dependencies are not as well-constrained.

4. Discussion

4.1. Relative IC 1613 – SMC – LMC Distances

With the availability of four independent distance measurements to IC 1613, we can attempt to determine relative distances between IC 1613 and the Magellanic Clouds. As the zero point subtracts out when measuring relative distances, this allows us, for the time being, to ignore the uncertainties in the calibrations. Table 4 and Figure 10 show these comparison values.

EDITOR: PLACE TABLE 4 HERE.

EDITOR: PLACE FIGURE 10 HERE.

For RR Lyraes, we adopt an absolute magnitude of $M_V = 0.60$ at [Fe/H] $= -1.3$. We conservatively adopt a metallicity dependence of 0.25 ± 0.10 magnitudes per dex, which is consistent with both the steep scale ($\frac{dM_V}{d[\mathrm{Fe/H}]} \sim 0.3$; for example, McNamara 1997) and the shallow scale ($\frac{dM_V}{d[\mathrm{Fe/H}]} \sim 0.2$; for example, Carretta et al. 2000), producing absolute magnitudes of $M_V = 0.58 \pm 0.01$ at [Fe/H] $= -1.4$ (NGC 121 in the SMC) and $M_V = 0.45 \pm 0.06$ at [Fe/H] $= -1.9$ (the clusters used for the LMC measurement). The resulting relative distances are shown in the first row of Table 4; we note that absolute distances would need to also include the zero point error of ± 0.15 magnitudes.

The Cepheid distance scale is based on the Madore & Freedman (1991) calibration, which assumes an LMC distance modulus of 18.50. This calibration does not include any metallicity dependence, a potential source of error given the significant metallicity range covered by these three objects (from [Fe/H] $\simeq -1.0$ for IC 1613 to [Fe/H] $\simeq -0.4$ for the LMC). As literature values for the dependence are more varied than are those for the RR Lyrae dependence, we will not attempt to make a correction here; instead the values in the second row of Table 4 assume no metallicity dependence.

Rows three and four of Table 4 similarly give RGB tip and red clump distances to the three objects. We adopt the Girardi et al. (2000) models to provide the absolute magnitudes of the RGB tips, and the Girardi & Salaris semi-empirical calibrations of the Magellanic Cloud red clump absolute magnitudes.

We note that both the relative IC 1613 − SMC distances and the relative IC 1613 − LMC distances are consistent between the four measurement methods. Using a weighted average of the four (by $\frac{1}{\sigma^2}$) relative IC 1613 − SMC distance measurements, we find a value of 5.44 ± 0.05, corresponding to a linear distance ratio of $\frac{d_{IC1613}}{d_{SMC}} = 12.2 \pm 0.3$. Because of the possible metallicity dependence in the Cepheids and the large metallicity difference between IC 1613 and the LMC, we average only the RR Lyrae, RGB tip, and red clump relative distances, finding a relative IC 1613 − LMC distance of 5.83 ± 0.06 (a linear distance ratio of $\frac{d_{IC1613}}{d_{LMC}} = 14.7 \pm 0.4$).

4.2. Metallicity Dependencies of Distance Indicators

Although the uncertainties are significant, we also wish to use the metallicity baseline in this comparison to examine the effects of metallicity on the RR Lyrae and Cepheid distance measurements. We first note that, since the four relative IC 1613 − LMC distance measurements are all consistent, our data are consistent with the metallicity dependencies adopted in the previous section: $\frac{dM_V}{d[\mathrm{Fe/H}]} = 0.25$ for RR Lyraes and $\frac{dM_V}{d[\mathrm{Fe/H}]} = \frac{dM_I}{d[\mathrm{Fe/H}]} = 0$ for Cepheids.

We first address the issue of the RR Lyrae metallicity dependence. Combining the red clump and RGB tip distances (which have both been corrected for population effects) to determine relative distances to the three objects, we derive reddening-corrected absolute magnitudes of $M_V(IC1613) = 0.61 \pm 0.08$, $M_V(SMC) = 0.58 \pm 0.08$, and

$M_V(LMC) = 0.41 \pm 0.10$. Fitting these values to a straight line (and adopting the metallicities from the previous section) with a least-χ^2 algorithm, we find a metallicity dependence of $\frac{dM_V}{d[\mathrm{Fe/H}]} = 0.34 \pm 0.20$ magnitudes per dex for the RR Lyrae absolute magnitude, a large value but consistent with more robust estimates of the metallicity dependency of the RR Lyrae absolute magnitudes (for example, Sandage et al. 1999, McNamara 1997, Layden et al. 1996, Carney, Storm, & Jones 1992, Sandage & Cacciari 1990, and Liu & Janes 1990). As our measured value has a large uncertainty, we will continue to use the adopted dependence of $\frac{dM_V}{d[\mathrm{Fe/H}]} = 0.25 \pm 0.10$ magnitudes per dex.

For the Cepheids, we adopt recent metallicities of [Fe/H] $\simeq -1.0$ for IC 1613 (based on an isochrone fit to these data), [Fe/H] $\simeq -0.8$ for the SMC (based on the cluster age-metallicity relation given by Olszewski, Suntzeff, & Mateo 1996), and [Fe/H] $\simeq -0.4$ for the LMC (also based on the cluster age-metallicity relation given by Olszewski et al. 1996). Following our procedure from the RR Lyrae dependence measurement, we will compare the Cepheid distances to those from the other distances (this time using the RR Lyrae, red clump, and RGB tip distances to measure the "true" distances). From the data in Table 4, we measure Cepheid $-$ "true" distances of 0.08 ± 0.14 for IC 1613, 0.03 ± 0.06 for the SMC, and 0.01 ± 0.05 for the LMC. A least-χ^2 fit to these points produces a metallicity dependence of -0.07 ± 0.16 magnitudes per dex in the Cepheid distances, consistent with zero or with the small metallicity dependencies determined empirically by Kennicutt et al. (1998) and theoretically by Sandage, Bell, & Tripicco (1999) and Alibert et al. (1999). Despite the large uncertainty, these data appear to rule out extreme values of the metallicity dependence, such as those of Caputo, Marconi, & Musella (2000), Beaulieu et al. (1997), and Gould (1994). We will adopt a conservative correction of -0.1 ± 0.2 magnitudes per dex, and correct the IC 1613 Cepheid distance (taken from Madore & Freedman 1991) to $\mu_0 = 24.34 \pm 0.18$. This value is still based on an assumed LMC distance modulus of 18.50, and adding an additional 0.1 magnitudes of uncertainty in that value produces our best IC

1613 Cepheid distance of $\mu_0 = 24.34 \pm 0.20$.

4.3. The Distance to IC 1613 and RR Lyrae Calibration

After applying the corrections above, we have four distance measurements to IC 1613, summarized in Table 5. Taking a weighted average (again weighting by $\frac{1}{\sigma^2}$), we measure the IC 1613 distance modulus to be $\mu_0 = 24.31 \pm 0.06$, corresponding to a distance of 730 ± 20 kpc. Although we have, in a sense, required the four distance measurements to be consistent in the previous section and thus have the possibility of circularity, we note that the RR Lyrae, RGB tip, and red clump distances are taken from section 3.3 (the RR Lyrae metallicity dependence measured above does not factor into the IC 1613 distance). Additionally, our weighted average of the distance measurements is 24.31 ± 0.06, whether or not the Cepheid distance is included (because of its high uncertainty). For completeness, we note that, had we used the Burstein & Heiles (1982) extinction maps instead of the Schlegel et al. (1998) maps, we would have used extinctions of $A_V = 0.02$ and $A_I = 0.01$, and arrived at a distance modulus of $\mu_0 = 24.36 \pm 0.06$.

EDITOR: PLACE TABLE 5 HERE.

We note that, given the accurate RGB tip and red clump measurements, we are able to work "backwards" to determine the RR Lyrae absolute magnitude. Removing the RR Lyrae distance from the weighted average, we arrive at an IC 1613 distance of $\mu_0 = 24.31 \pm 0.07$. Combining this with our reddening-corrected mean magnitude of $V_0 = 24.92 \pm 0.04$, we calculate the absolute magnitude of IC 1613 RR Lyraes to be 0.61 ± 0.08.

5. Summary

We have presented photometry, variable star analysis, and a series of distance measurements of a WFPC2 field in the halo of IC 1613. We found thirteen RR Lyrae stars and a mean extinction-corrected magnitude of $\langle V \rangle_0(RR) = 24.92 \pm 0.04$. The presence of these stars confirms the existence of an old horizontal branch, consistent with the ground-based results of Saha et al. (1992). We also found eleven short-period Cepheids, two of which were fundamental mode with sufficiently long periods to determine a distance. Finally, we applied RGB tip and red clump distance measurements to IC 1613, determining distances for each. The summary of our values is given in Table 5, along with the primary sources of error in those four measurement.

We assume that the RGB tip distance is the most robust of the four, given that the dependencies on age and metallicity are very small and have been calibrated. However, the small field of view of WFPC2 limits our ability to accurately measure the position of the tip, limiting the accuracy of our measurement to $\mu_0(RGB) = 24.32 \pm 0.09$. The red clump distance, on the other hand, has significant calibration uncertainty based on the age dependence, but its position can be accurately measured in these data. Adding the population-dependencies into our uncertainties, we find a red clump distance of $\mu_0(RC) = 24.30 \pm 0.09$.

Our sample of Cepheids was insufficient to produce an accurate distance measurement, but we were able to confirm that our two ~ 3 day fundamental-mode Cepheids were consistent with the Cepheid distance obtained by Madore & Freedman (1991). We were also able to estimate, via comparisons with LMC and SMC distances, a metallicity dependence of -0.07 ± 0.16 magnitudes per dex. Applying a conservative estimate of the metallicity dependence (-0.1 ± 0.2 magnitudes per dex) and an extinction of $A_V = 0.08$ from Schlegel et al. (1998) to the Madore & Freedman (1991) produces a corrected IC 1613 Cepheid

distance modulus of $\mu_0(Ceph) = 24.34 \pm 0.20$. Combining this with our other distance measurements with a weighted average, we arrive at our best IC 1613 distance modulus of $\mu_0 = 24.31 \pm 0.06$, corresponding to a distance of 730 ± 20 kpc.

A similar treatment was given to the RR Lyrae, producing a metallicity dependence of 0.34 ± 0.20 magnitudes per dex in the V absolute magnitude, consistent with literature values. Given the wide variety of RR Lyrae absolute magnitudes in the literature, we also found it useful to measure the IC 1613 RR Lyrae absolute magnitude, given our observed mean V magnitude and the distances calculated through other measurements. We calculated a mean M_V of 0.61 ± 0.08 at [Fe/H] $\simeq -1.3$, a value consistent with both the "faint" calibration of Fernley et al. (1998) and the "bright" calibration of Gratton et al. (1997).

We note that, when each distance measurement is properly calibrated and corrected for population effects, the RR Lyrae, Cepheid, RGB tip, and red clump distance techniques produce consistent relative distances between IC 1613 and the Magellanic Clouds. We find a relative IC 1613 − SMC distance modulus of 5.44 ± 0.05 and a relative IC 1613 − LMC distance modulus of 5.83 ± 0.06. We also note that all four distance indicators produce consistent distances to IC 1613.

Support for this work was provided by NASA through grant numbers GO-07496 and GO-02227.06-A from the Space Telescope Science Institute, which is operated by AURA, Inc., under NASA contract NAS 5-26555. EDS is grateful for partial support from NASA LTSARP grants No. NAGW-3189 and NAG5-9221.

REFERENCES

Alibert, Y., Baraffe, I., Hauschildt, P., & Allard, F. 1999, A&A, 344, 551

Antonello, E., Mantegazza, L., Fugazza, D., Bossi, M., & Covino, S. 1999, A&A, 349, 55

Bauer, F. et al. 1999, A&A, 348, 175

Beaulieu, J. P. et al. 1997, A&A, 318, L47

Burstein, D. & Heiles, C. 1982, AJ, 87, 1165

Caloi, V., D'Antona, F., & Mazzitelli, I. 1997, A&A, 320, 823

Caputo, F., Castellani, V., Marconi, M., & Ripepi, V. 2000, MNRAS, 316, 819

Caputo, F., Marconi, M., & Musella, I. 2000, A&A, 354, 610

Carney, B. W., Storm, J., Jones, R. V. 1992, ApJ, 386, 663

Carretta, E. & Gratton, R. G., A&AS, 121, 95

Carretta, E., Gratton, R. G., Clementini, G., & Fusi Pecci, F. 2000, ApJ, 533, 215

Cassisi, S., Castellani, V., Degl'Innocenti, S., Salaris, M., & Weiss, A. 1999, A&AS, 134, 103

Castellani, V. & Degl'Innocenti, S. 1999, A&A, 344, 97

Cioni, M.-R. L., van der Marel, R. P., Loup, C., & Habing, H. J. 2000, A&A, 359, 601

Cole, A. A. et al. 1999, AJ, 118, 1657

Demarque, P., Zinn, R., Lee, Y.-W., & Yi, S. 2000, AJ, 119, 1398

Dolphin, A. E. 2000a, PASP, in press

Dolphin, A. E. 2000b, PASP, in press

Fernley, J., Barnes, T. G., Skillen, I., Hawley, S. L., Hanley, C. J., Evans, D. W., Solano, E., & Garrido, R. 1998, A&A, 330, 515

Freedman, W. L. 1988, ApJ, 326, 691

Girardi, L., Bressan, A., Bertelli, G., & Chiosi, C. 2000, A&AS, 141, 371

Girardi, L., Groenewegen, M. A. T., Weiss, A., & Salaris, M. 1998, MNRAS, 301, 149

Girardi, L., & Salaris, M. 2000, MNRAS, in press

Gould, A. 1994, ApJ, 426, 542

Gratton, R. G., Fusi Pecci, F., Carretta, E., Clementini, G., Corsi, C. E., & Lattanzi, M. 1997, ApJ, 491, 749

Holtzman, J. A. et al. 1999, AJ, 118, 2262

Kennicutt, R. C. et al. 1998, ApJ, 498, 181

Labhardt, L., Sandage, A., & Tammann, G. A. 1997, A&A, 322, 751

Lafler, J., & Kinman, T. D. 1965, ApJS, 11, 216

Lake, G. R., & Skillman, E. D. 1989, AJ, 98, 1274.

Laney, C. D., & Stobie, R. S. 1994, MNRAS, 266, 441

Layden, A. C., Hanson, R. B., Hawley, S. L., Klemora, A. R., & Hanley, C. J. 1996, AJ, 112, 2110

Lee, M. G., Freedman, W. L., & Madore, B. F. 1993, ApJ, 417, 553

Liu, T., & Janes, K. A. 1990, ApJ, 354, 273

Madore, B. F., & Freedman, W. L. 1991, PASP, 103, 933

Mantegazza, L., & Poretti, E. 1992, A&A, 261, 137

Mateo, M. 1998, ARA&A, 36, 435

McAlary, C. W., Madore, B. F., & Davis, L. E. 1984, ApJ, 276, 487

McNamara, D. H. 1997, PASP, 109, 857

Olson, K. A. G. 1999, AJ, 117, 2244

Olszewski, E. W., Suntzeff, N. B., & Mateo, M. 1996, ARA&A, 35, 511

Paczynski, B. & Stanek, K. Z. 1998, ApJ, 494

Rocha-Pinto, H. J., Maciel, W. J., Scalo, J., & Flynn, C. 2000, A&A, 358, 850

Saha, A., Freedman, W. L., Hoessel, J.G., & Mossman, A. E. 1992, AJ, 104, 1072

Saha, A., & Hoessel, J. G. 1987, AJ, 94, 1556

Saha, A., & Hoessel, J. G. 1990, AJ, 99, 97

Saha, A., Sandage, A., Labhardt, L., Tammann, G. A., Macchetto, F. D., & Panagia, N. 1996, ApJ, 466, 55

Sakai, S., Zaritsky, D., & Kennicutt, R. C. 2000, AJ, 119, 1197

Salaris, M. & Cassisi, S. 1998, MNRAS, 298, 166

Sandage, A. 1971, ApJ, 166, 13

Sandage, A., Bell, R. A., & Tripicco, M. J. 1999, ApJ, 522, 250

Sandage, A., & Cacciari, C. 1990, ApJ, 350, 645

Sarajedini, A. 1999, AJ, 118, 2321

Schlegel, D. J., Finkbeiner, D. P., & Davis, M. 1998, ApJ, 500, 525

Stanek, K. Z. & Garnavich, P. M. 1998, AAS meeting 193, 106.05

Talent, D. L. 1980, Ph.D. Thesis, Rice University

Tolstoy, E. 1999, Ap&SS, 265, 199

Udalski, A. 2000, ApJ, 531, L25

van den Bergh, S. 2000, *The Galaxies of the Local Group*, Cambridge: Cambridge University Press

Walker, A. 1992, ApJ, 390, 81

Walker, A., & Mack, A. R. 1988, AJ, 96, 872

Zinn, R. & West, M. J. 1984, ApJS, 55, 45

This manuscript was prepared with the AAS LaTeX macros v4.0.

Fig. 1.— F814W WFPC2 image of IC 1613 field, combined from 8 1200s exposures

Fig. 2.— $(V - I)$, I Color-magnitude diagram (12983 stars), calculated from mean magnitudes in all epochs. Poorly-fit stars ($\chi > 1.5$ or |sharpness| > 0.3) are not included. Error bars show typical $(V - I)$ uncertainties as a function of I. Absolute magnitudes (on the y-axis on the right) are calculated assuming $I - M_I = 24.36$.

Fig. 3.— Photometry accuracy for the IC 1613 data. Values given are magnitudes at individual epochs minus mean magnitudes. The locations of the Cepheids (F555W of $\sim 22 - 23$) and RR Lyraes (F555W of ~ 25) are shown by the excess scatter, and the limiting accuracy of 0.015 magnitudes at the bright end is clear.

Fig. 4.— CMD of IC 1613 field, showing the periodic variable stars. Circles are the Cepheids, diamonds the RR Lyraes, and triangles the two possible eclipsing binaries. The detection efficiency was not 100%, and thus there are many stars in the instability strip. Absolute magnitudes (on the y-axis on the right) are calculated assuming $I - M_I = 24.36$.

Fig. 5.— Light curves of 13 candidate RR Lyraes.

Fig. 6.— Light curves of 11 candidate Cepheids.

Fig. 7.— Cepheid period-luminosity relation. Solid circles are fundamental pulsators, open circles are overtone pulsators, and crosses are the Cepheids found by Freedman (1988). All but one of the Cepheids were classified by light curve shape. The solid lines are mean P-L relations from Madore & Freedman (1991), with a distance modulus of 24.45 and extinction of $A_V = 0.08$. The dashed line is the break at P=2 days, based on Bauer et al. (1999)

Fig. 8.— I-band luminosity function along the RGB. Our measured TRGB is at $I = 20.35 \pm 0.07$, and is marked by the vertical line at that position.

Fig. 9.— I-band luminosity function for stars with $0.8 \leq V - I \leq 0.95$ and $22 \leq I \leq 25.5$. The line is the best fit, using a quadratic polynomial to fit the RGB and a Gaussian to fit the red clump.

Fig. 10.— Distance modulus differences between IC 1613 and the Magellanic Clouds, using four distance measurements. The top panel shows the IC 1613 - SMC differences and the bottom panel the IC 1613 - LMC differences. We note that all four distance measurement techniques produce consistent distance ratios.

Table 1. RR Lyraes

ID	chip	X	Y	$\langle V \rangle$	$\langle V-I \rangle$	period	Q
V5	WFC2	174.01	582.68	25.222 ± 0.087	0.678 ± 0.097	0.59	3
V8	WFC2	498.73	101.37	24.948 ± 0.039	0.333 ± 0.051	0.50	2
V14	WFC3	368.24	153.10	25.098 ± 0.083	0.345 ± 0.092	0.31	3
V15	WFC3	447.66	154.61	25.077 ± 0.056	0.554 ± 0.067	0.63	3
V16	WFC3	519.91	703.76	25.097 ± 0.068	0.463 ± 0.074	0.34	2
V17	WFC3	559.79	569.96	24.790 ± 0.102	0.410 ± 0.111	0.62	3
V18	WFC3	599.32	495.63	24.971 ± 0.085	0.501 ± 0.090	0.65	4
V19	WFC3	661.68	400.55	25.233 ± 0.152	0.368 ± 0.170	0.43	4
V20	WFC3	770.59	790.22	24.728 ± 0.135	0.287 ± 0.142	0.61	2
V21	WFC4	343.38	584.32	24.987 ± 0.120	0.529 ± 0.132	0.60	4
V22	WFC4	585.38	573.20	25.058 ± 0.091	0.550 ± 0.107	0.58	2
V23	WFC4	610.83	108.18	24.843 ± 0.112	0.406 ± 0.121	0.39	4
V24	WFC4	691.07	215.75	24.890 ± 0.053	0.707 ± 0.094	0.48	2

Table 2. Cepheids

ID	chip	X	Y	$\langle V \rangle$	$\langle I \rangle$	period	mode	Q
V1	WFC1	290.70	582.93	22.103 ± 0.064	21.650 ± 0.049	1.67 ± 0.17	OT	2
V2	WFC2	120.54	360.19	22.584 ± 0.059	21.990 ± 0.024	1.31 ± 0.05	OT	4
V3	WFC2	133.33	429.22	21.802 ± 0.120	21.211 ± 0.060	3.31 ± 0.06	FM	4
V4	WFC2	146.33	595.41	22.606 ± 0.074	22.040 ± 0.051	1.09 ± 0.08	OT	3
V6	WFC2	387.65	282.16	21.548 ± 0.162	21.083 ± 0.090	3.03 ± 0.05	FM	4
V7	WFC2	482.48	424.66	23.006 ± 0.093	22.455 ± 0.065	1.34 ± 0.06	FM	4
V9	WFC2	505.88	94.89	22.675 ± 0.110	22.095 ± 0.076	1.75 ± 0.06	FM	4
V10	WFC2	552.35	83.57	23.144 ± 0.150	22.627 ± 0.071	1.05 ± 0.03	FM	3
V13	WFC3	366.95	129.45	21.403 ± 0.045	20.760 ± 0.030	2.82 ± 1.20	OT	3
V25	WFC4	716.29	460.78	22.565 ± 0.147	22.206 ± 0.051	0.95 ± 0.05	OT	4
V26	WFC4	717.22	589.95	22.769 ± 0.050	22.211 ± 0.032	1.00 ± 0.07	OT	3

Table 3. Cepheid Distances

ID	$\langle V \rangle_0$	$\langle I \rangle_0$	period	M_V	M_I	μ_0
V3	21.80 ± 0.12	21.15 ± 0.06	3.31 ± 0.06	-2.83 ± 0.27	-3.40 ± 0.18	24.58 ± 0.21
V6	21.55 ± 0.16	21.08 ± 0.09	3.03 ± 0.05	-2.73 ± 0.27	-3.28 ± 0.18	24.33 ± 0.21

Table 4. IC 1613, SMC, and LMC Distance Moduli

Method	IC 1613	SMC	IC 1613 - SMC	LMC	IC 1613 - LMC
RR Lyrae	24.32 ± 0.05[a]	18.88 ± 0.07[b]	5.44 ± 0.09	18.49 ± 0.07[c]	5.83 ± 0.09
Cepheid	24.40 ± 0.13[d]	18.91 ± 0.04[e]	5.49 ± 0.14	18.50 ± 0.00[f]	5.90 ± 0.13
RGB Tip	24.32 ± 0.07[g]	18.90 ± 0.04[h]	5.42 ± 0.08	18.57 ± 0.09[i]	5.82 ± 0.11
Red Clump	24.30 ± 0.09	18.85 ± 0.06[j]	5.45 ± 0.11	18.46 ± 0.11[k]	5.84 ± 0.14

[a]Adopting $M_V(RR) = 0.60$. For this and all other distances in this table, calibration uncertainties are assumed to be zero because we are only interested in measuring relative distances.

[b]From Walker & Mack (1988) for NGC 121 ([Fe/H] $= -1.4$), adopting $M_V(RR) = 0.58 \pm 0.02$.

[c]From Walker (1992) for clusters with mean [Fe/H] $= -1.9$, adopting $M_V(RR) = 0.45 \pm 0.06$.

[d]From Madore & Freedman (1991), adjusting to our extinction of $A_V = 0.08$.

[e]Laney & Stobie (1994), adopting an LMC distance modulus of 18.50

[f]LMC distance modulus of 18.50 is assumed in calibration of IC 1613 and SMC distances

[g]Adopting $M_I(TRGB) = -4.02$

[h]From Cioni et al. (2000), adopting $M_I(TRGB) = -4.02$ and $A_I = 0.07$ based on Schlegel et al. (1998)

[i]From Sakai, Zaritsky, & Kennicutt (2000), adopting $M_I(TRGB) = -4.03$ calculated from the Girardi et al. (2000) models

[j]From Girardi & Salaris (2000)

[k]From Girardi & Salaris (2000), adopting the mean of their two possible values

Table 5. IC 1613 Distance Moduli

Method	This Work	Primary source of error	Best Value
RR Lyrae	24.32 ± 0.16	M_V vs. [Fe/H] calibration	24.32 ± 0.16
Cepheid	24.45 ± 0.15	Small number (2)	24.34 ± 0.20
RGB Tip	24.32 ± 0.09	Measurement	24.32 ± 0.09
Red Clump	24.30 ± 0.09	Age effects	24.30 ± 0.09
Combined			24.31 ± 0.06

This figure "fig01.jpg" is available in "jpg" format from:

http://arXiv.org/ps/astro-ph/0012150v1

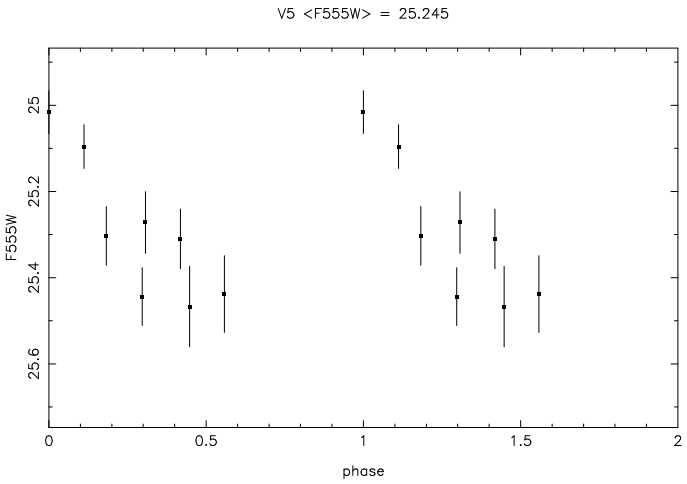
V5 <F555W> = 25.245
F555W
25
25.2
25.4
25.6
0
0.5
1
1.5
2
phase

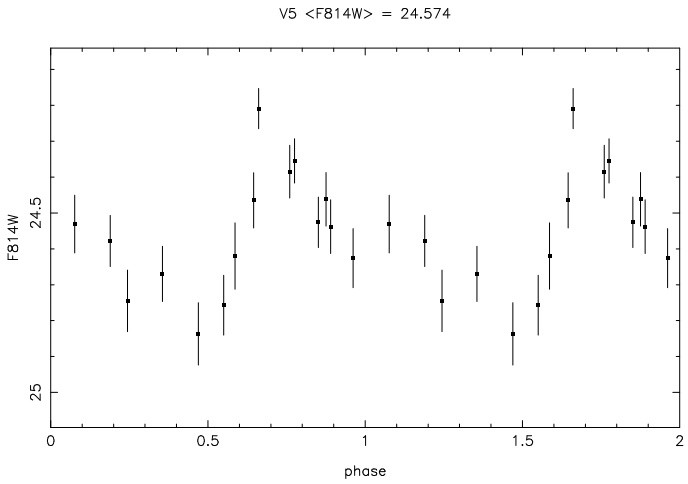
V5 <F814W> = 24.574
F814W
24.5
25
0
0.5
1
1.5
2
phase

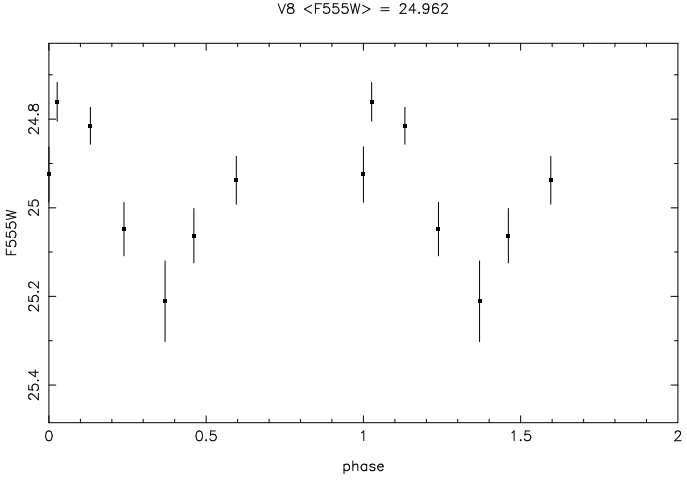
V8 <F555W> = 24.962
F555W
24.8
25
25.2
25.4
0
0.5
1
1.5
2
phase

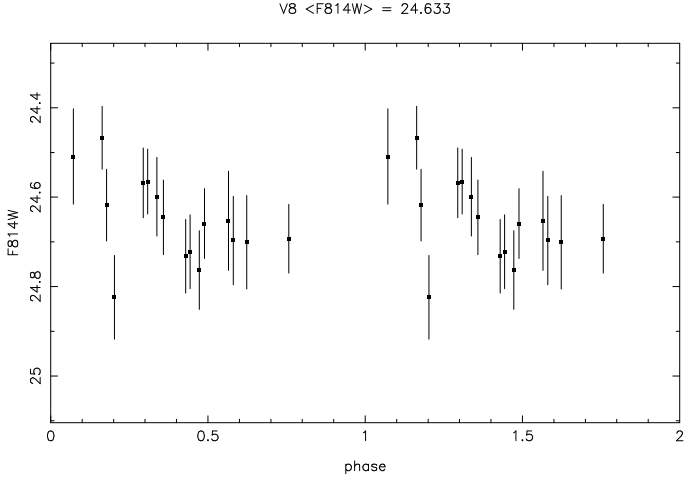
V8 <F814W> = 24.633
F814W
24.4
24.6
24.8
25
0
0.5
1
1.5
2
phase

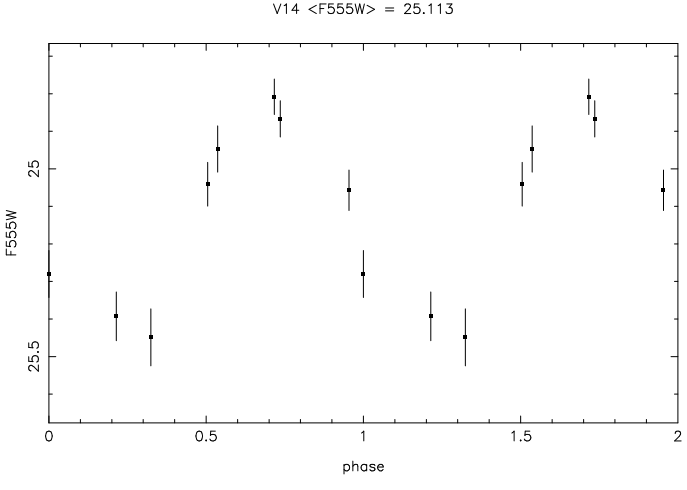
V14 <F555W> = 25.113
F555W
25
25.5
0
0.5
1
1.5
2
phase

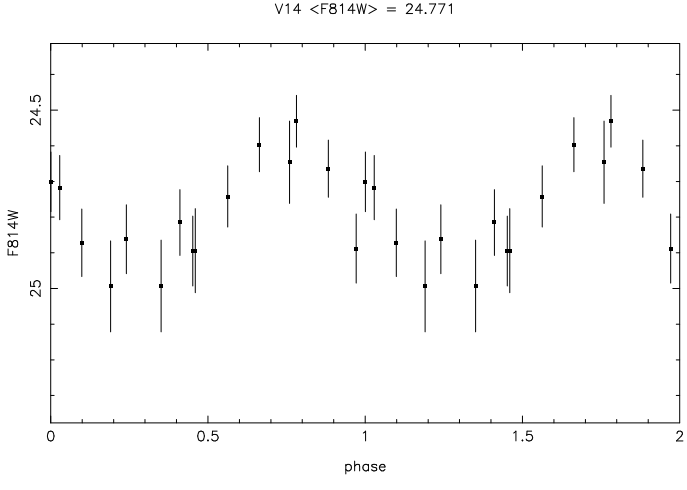
V14 <F814W> = 24.771
F814W
24.5
25
0
0.5
1
1.5
2
phase

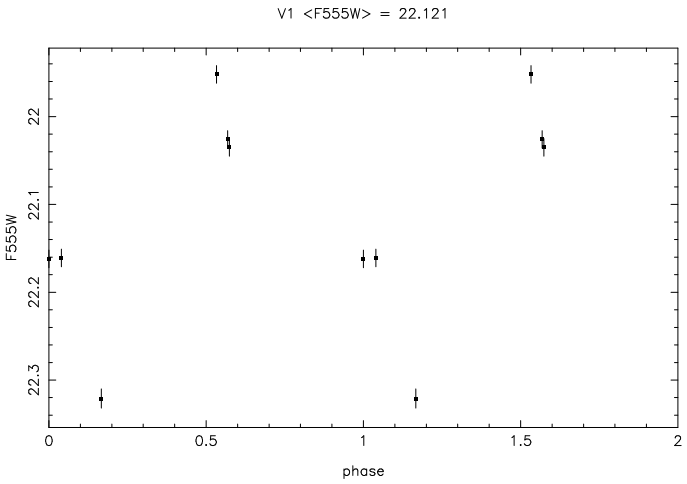
V1 <F555W> = 22.121
F555W
phase

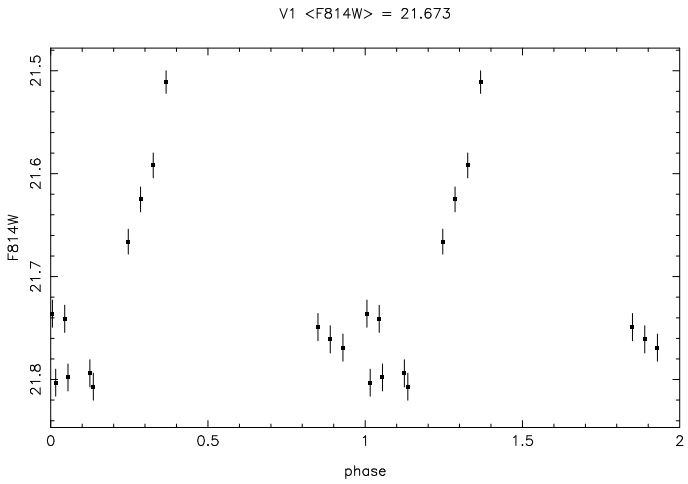
V1 <F814W> = 21.673
F814W
phase

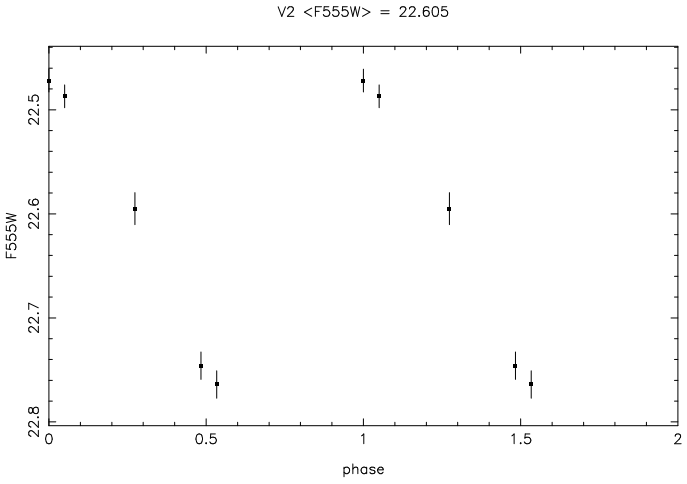
V2 <F555W> = 22.605
F555W
phase

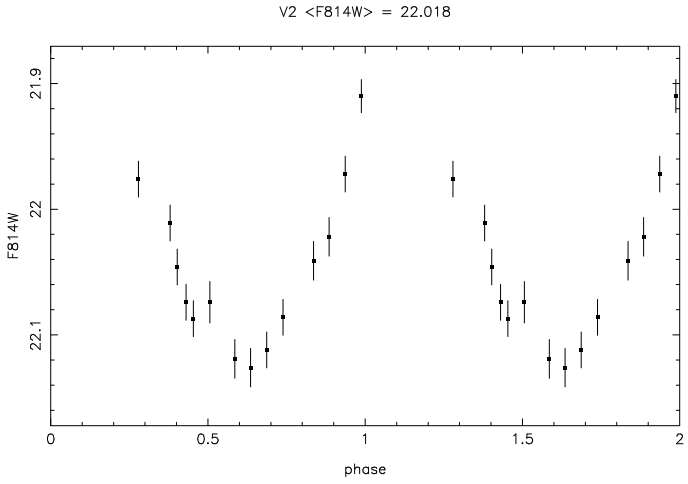
V2 <F814W> = 22.018
F814W
phase

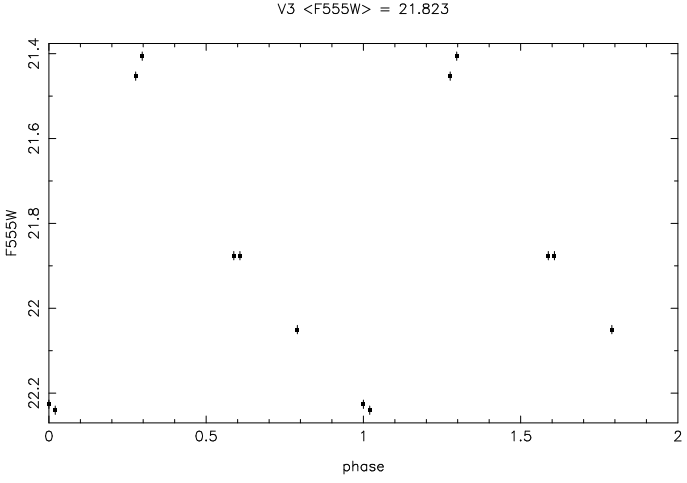
V3 <F555W> = 21.823
F555W
phase

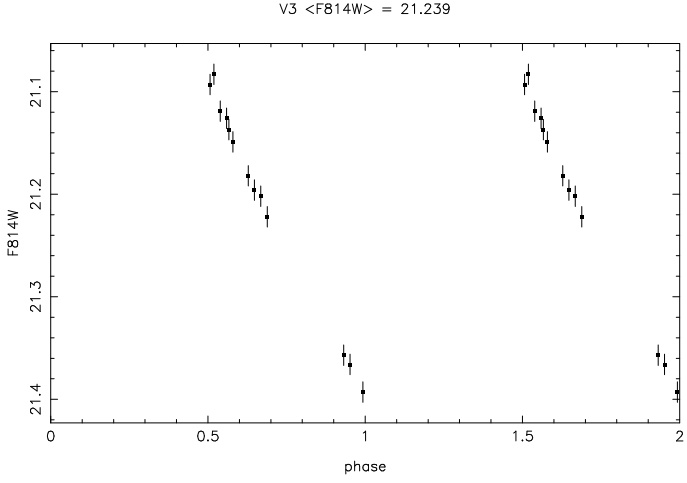
V3 <F814W> = 21.239
F814W
phase

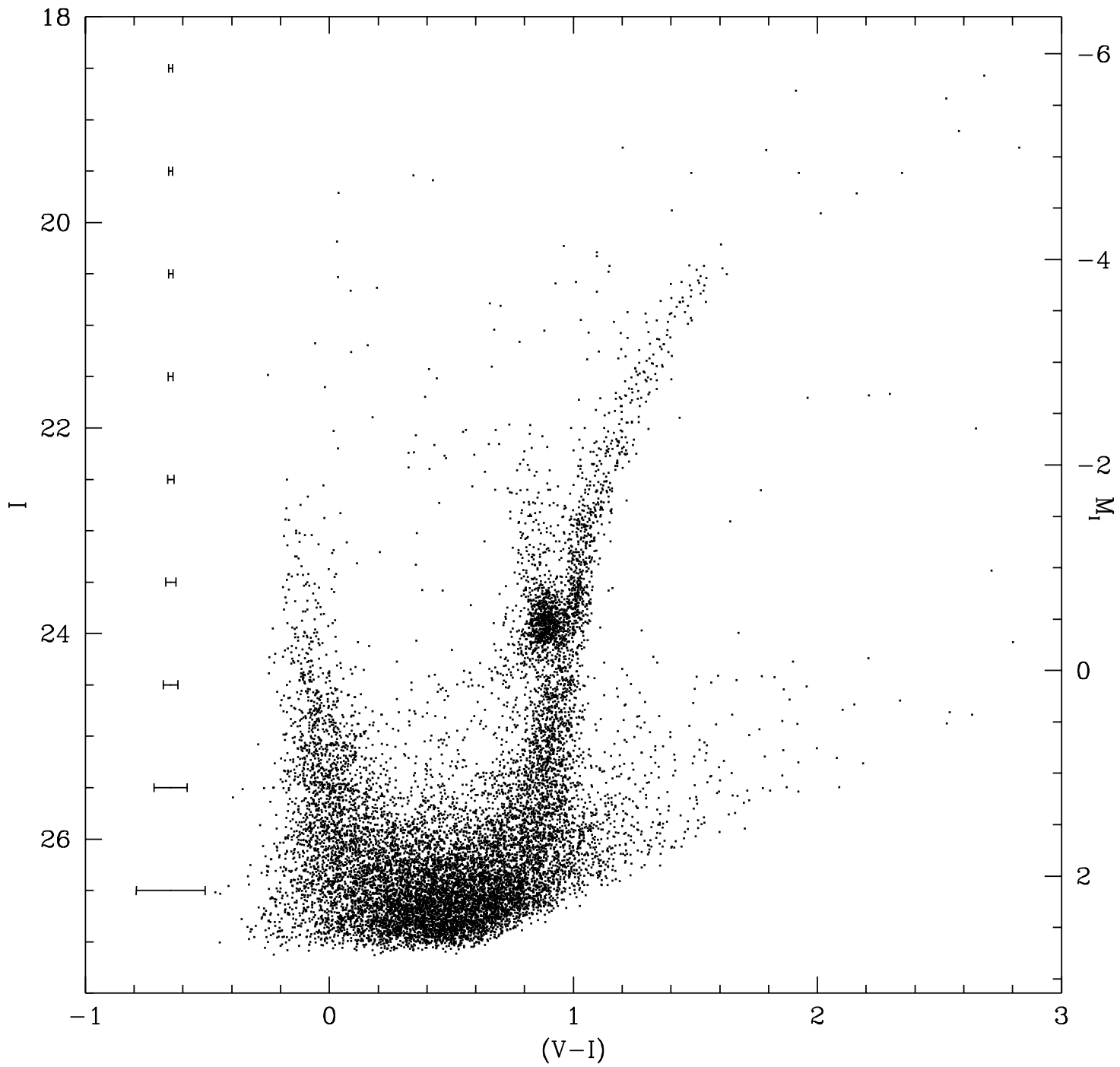
18
20
22
24
26
I
−6
−4
−2
0
2
M_I
−1
0
1
2
3
(V−I)

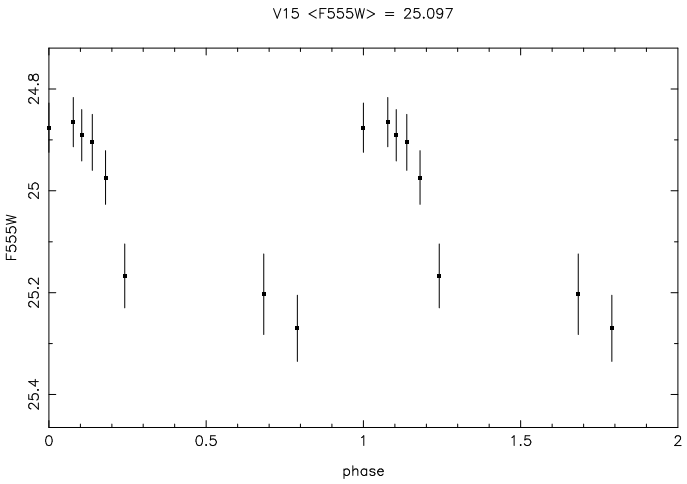
V15 <F555W> = 25.097
F555W
phase

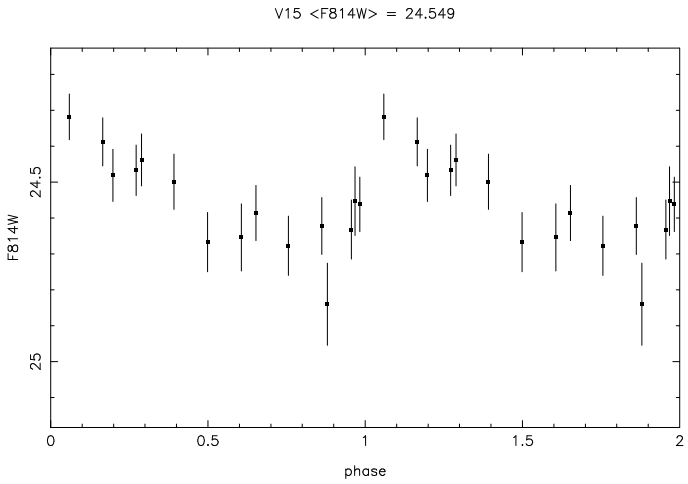
V15 <F814W> = 24.549
F814W
phase

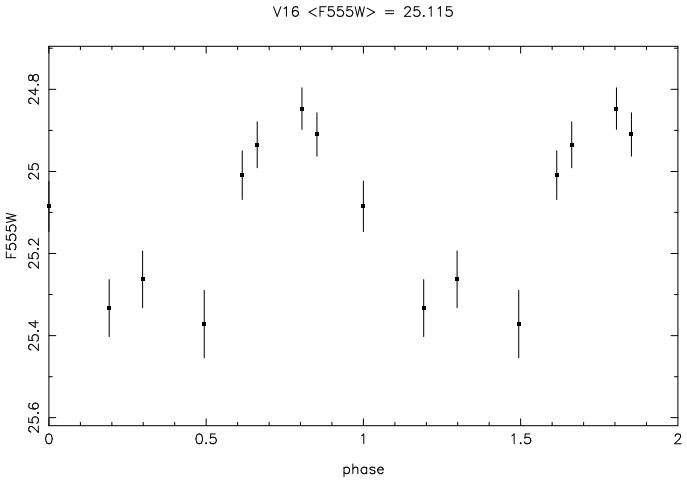
V16 <F555W> = 25.115
F555W
phase

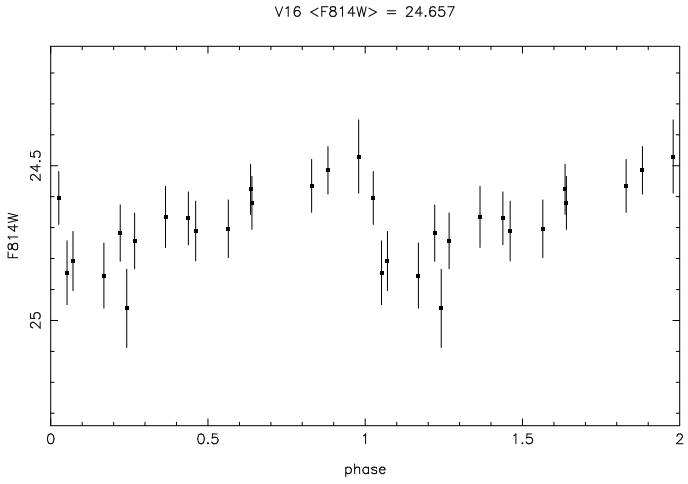
V16 <F814W> = 24.657
F814W
phase

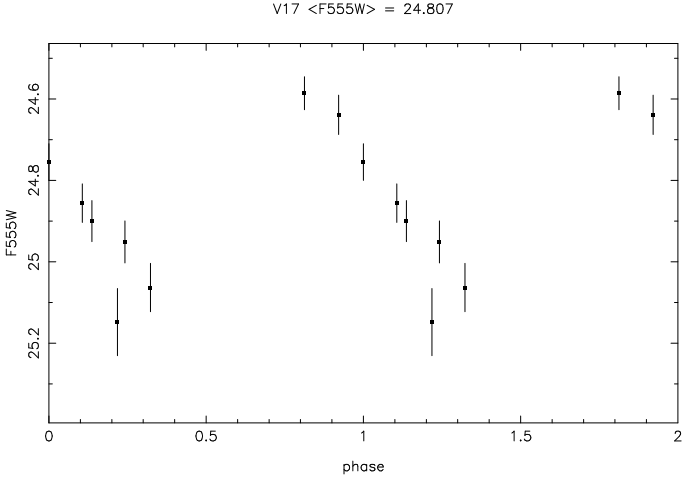
V17 <F555W> = 24.807
F555W
phase

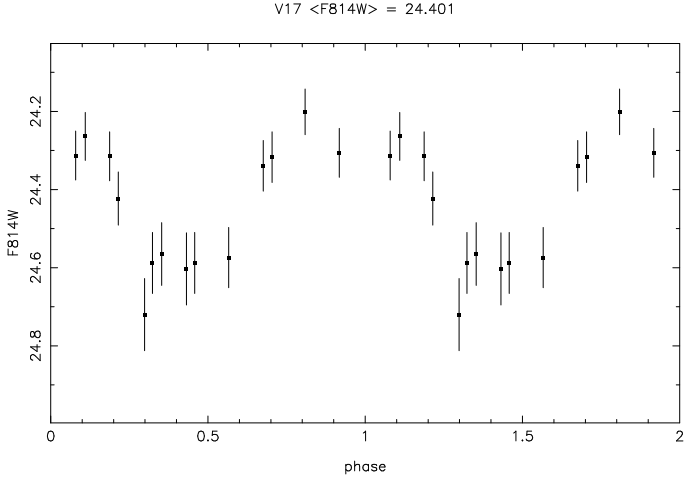
V17 <F814W> = 24.401
F814W
phase

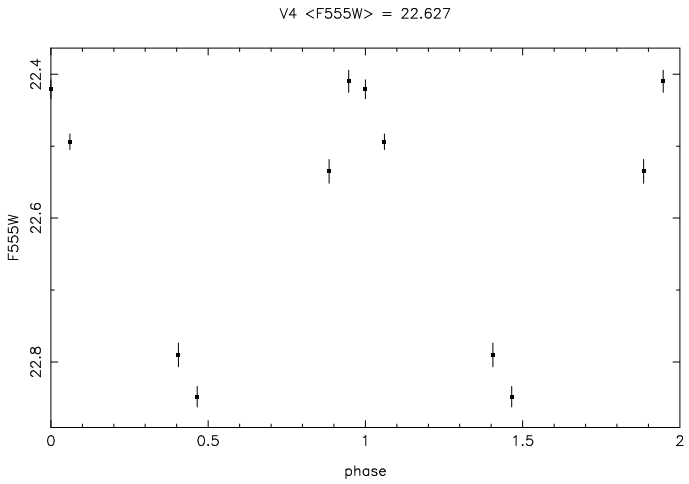
V4 <F555W> = 22.627
F555W
22.4
22.6
22.8
0
0.5
1
1.5
2
phase

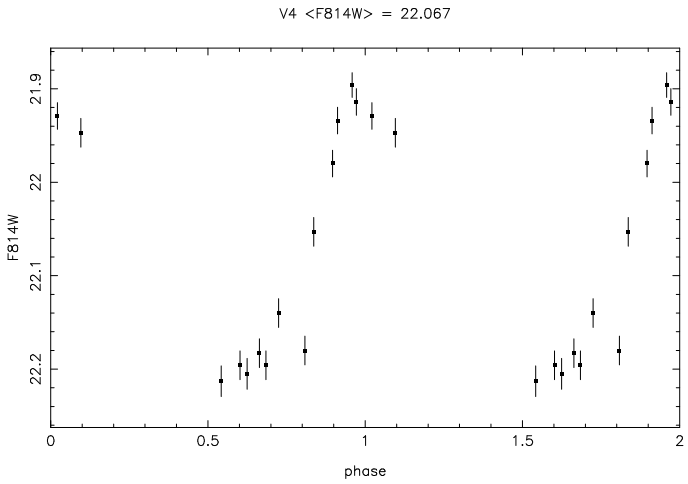
V4 <F814W> = 22.067
F814W
21.9
22
22.1
22.2
0
0.5
1
1.5
2
phase

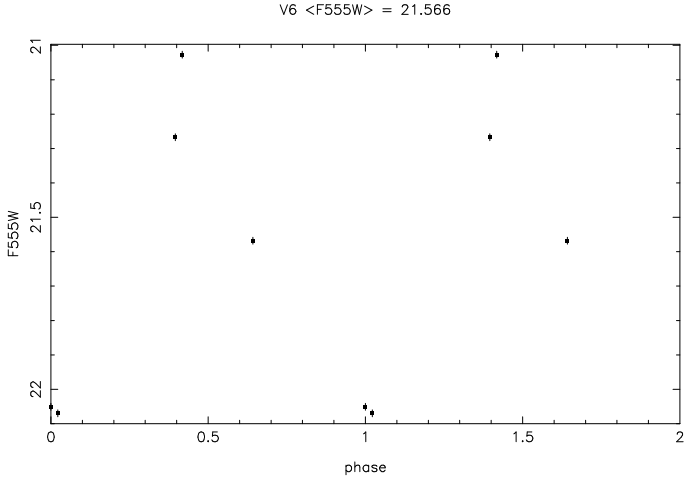
V6 <F555W> = 21.566
F555W
21
21.5
22
0
0.5
1
1.5
2
phase

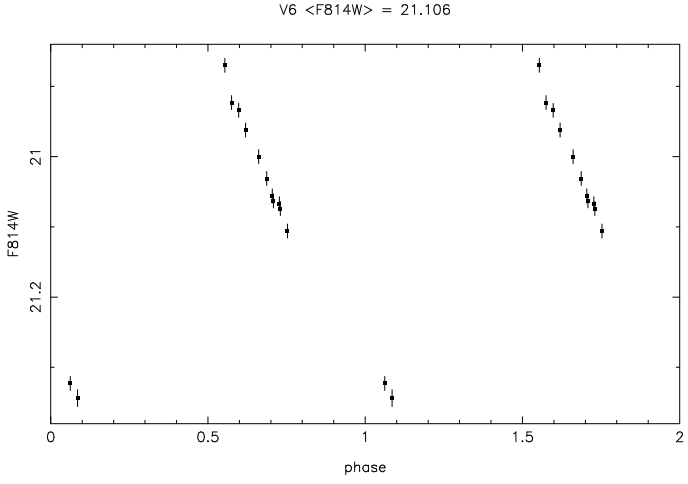
V6 <F814W> = 21.106
F814W
21
21.2
0
0.5
1
1.5
2
phase

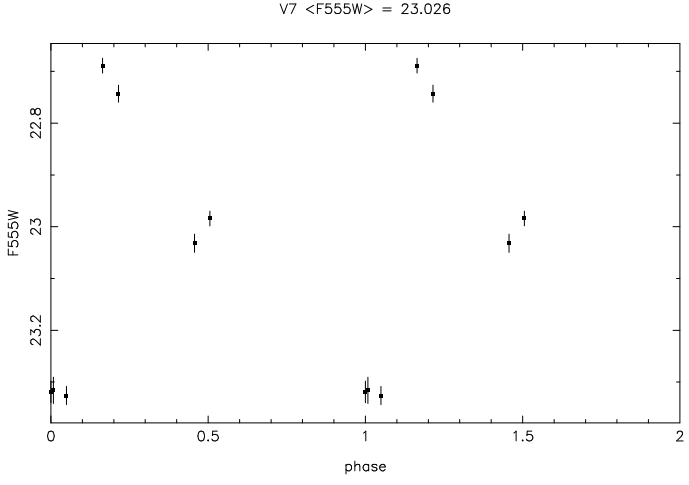
V7 <F555W> = 23.026
F555W
22.8
23
23.2
0
0.5
1
1.5
2
phase

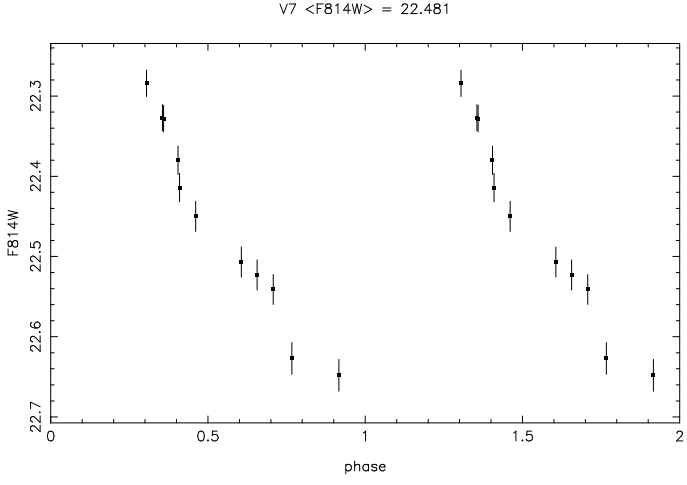
V7 <F814W> = 22.481
F814W
22.3
22.4
22.5
22.6
22.7
0
0.5
1
1.5
2
phase

This figure "fig03.jpg" is available in "jpg" format from:

http://arXiv.org/ps/astro-ph/0012150v1

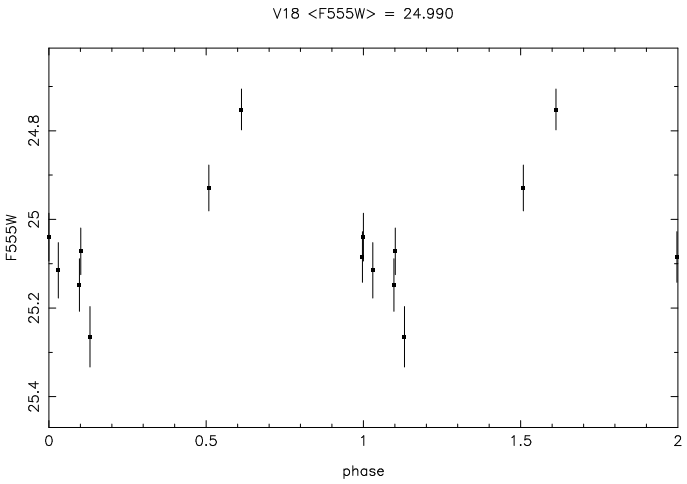
V18 <F555W> = 24.990
F555W
phase

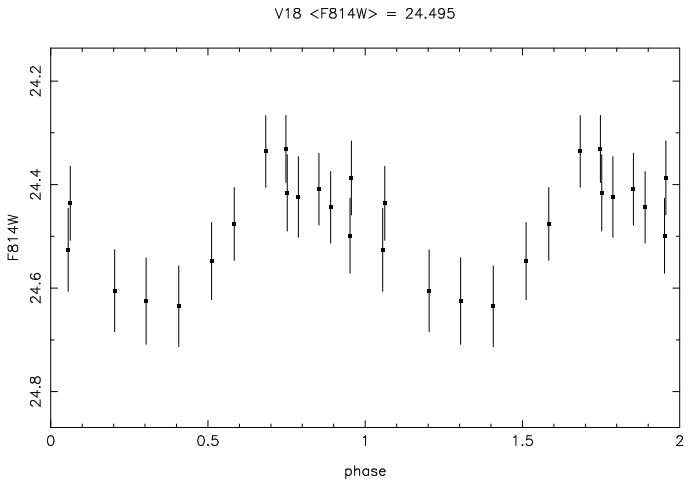
V18 <F814W> = 24.495
F814W
phase

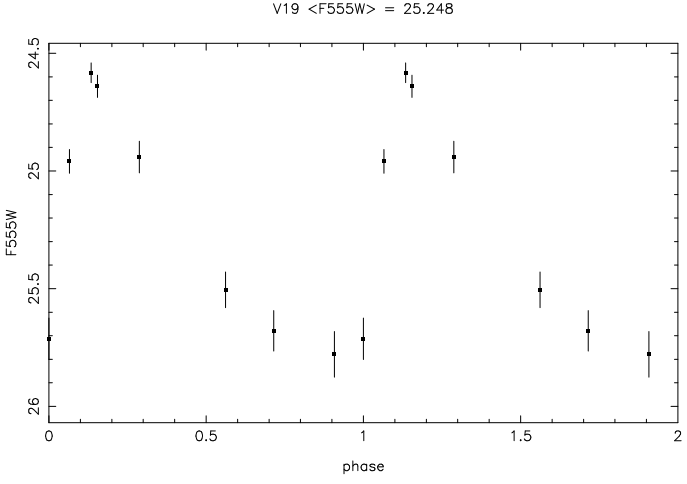
V19 <F555W> = 25.248
F555W
phase

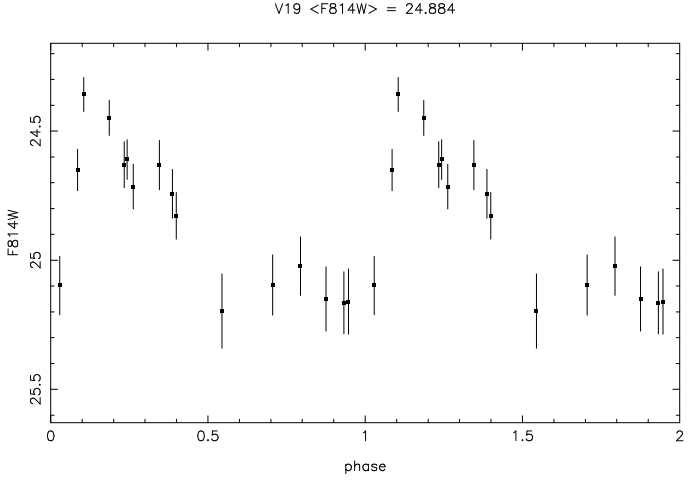
V19 <F814W> = 24.884
F814W
phase

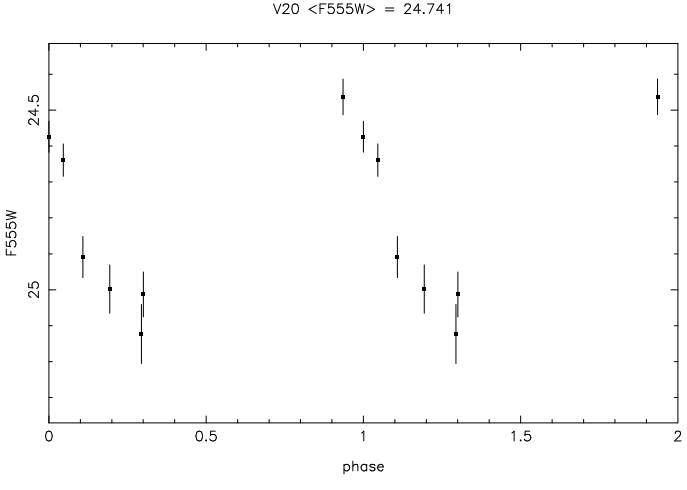
V20 <F555W> = 24.741
F555W
phase

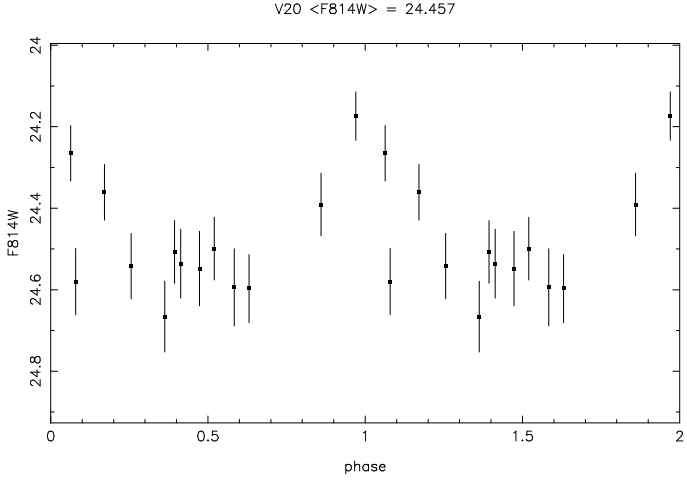
V20 <F814W> = 24.457
F814W
phase

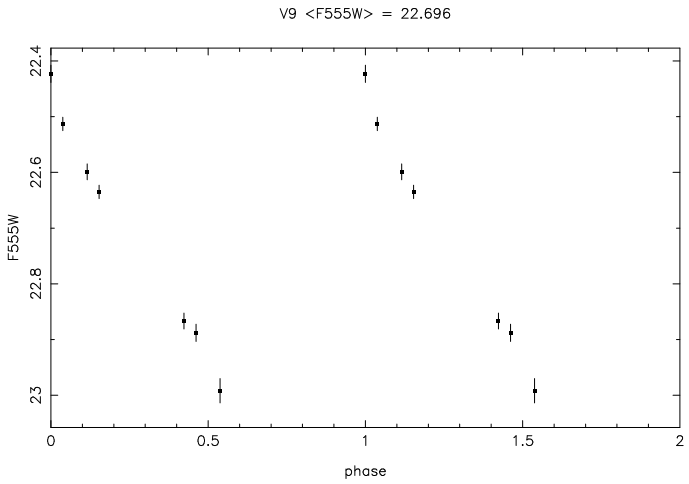
V9 <F555W> = 22.696
F555W
22.4
22.6
22.8
23
0
0.5
1
1.5
2
phase

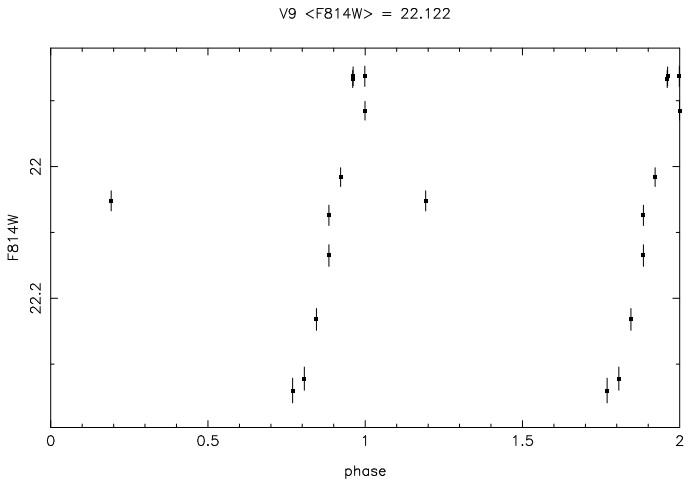
V9 <F814W> = 22.122
F814W
22
22.2
0
0.5
1
1.5
2
phase

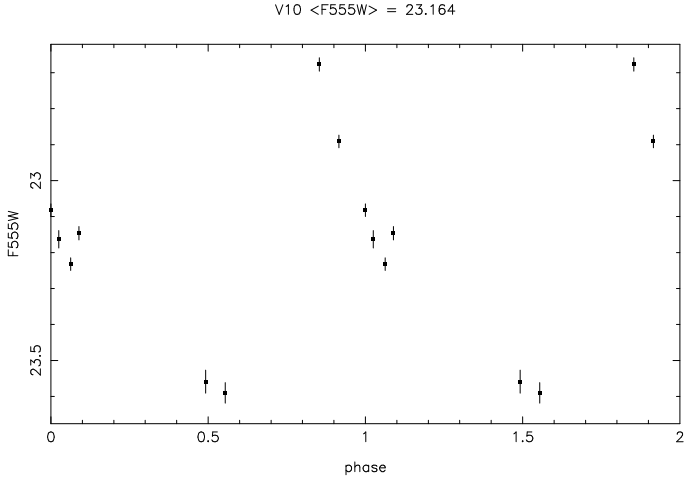
V10 <F555W> = 23.164
F555W
23
23.5
0
0.5
1
1.5
2
phase

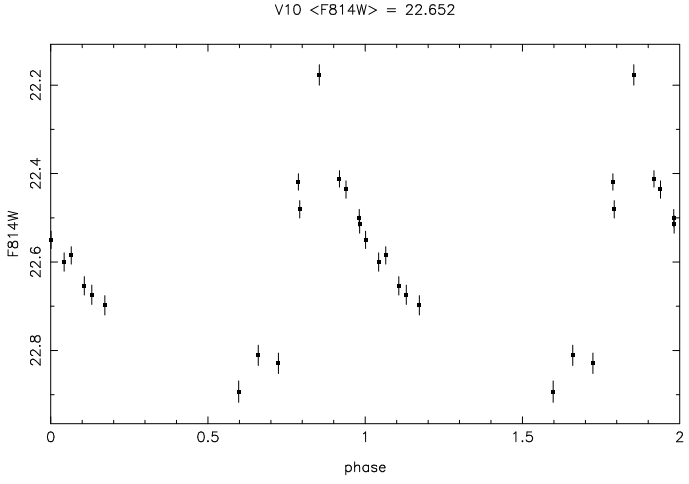
V10 <F814W> = 22.652
F814W
22.2
22.4
22.6
22.8
0
0.5
1
1.5
2
phase

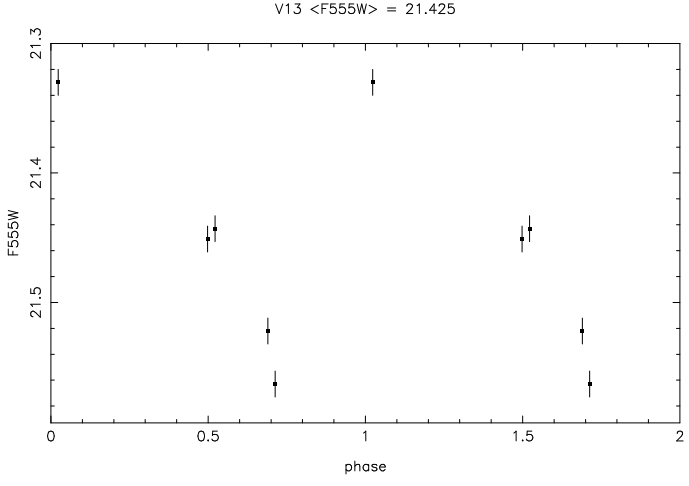
V13 <F555W> = 21.425
F555W
21.3
21.4
21.5
0
0.5
1
1.5
2
phase

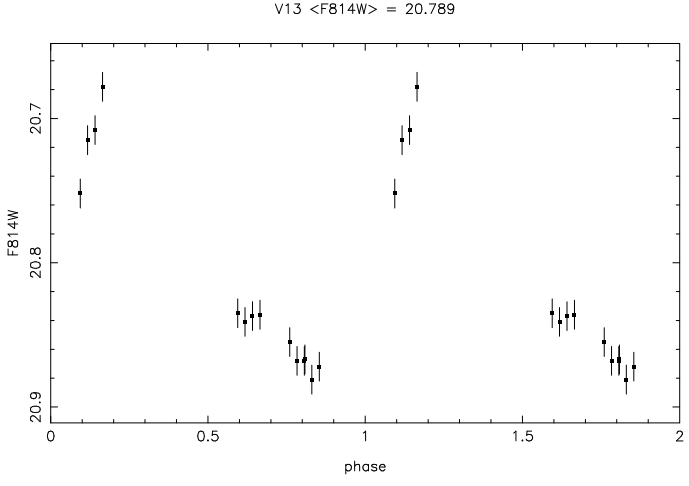
V13 <F814W> = 20.789
F814W
20.7
20.8
20.9
0
0.5
1
1.5
2
phase

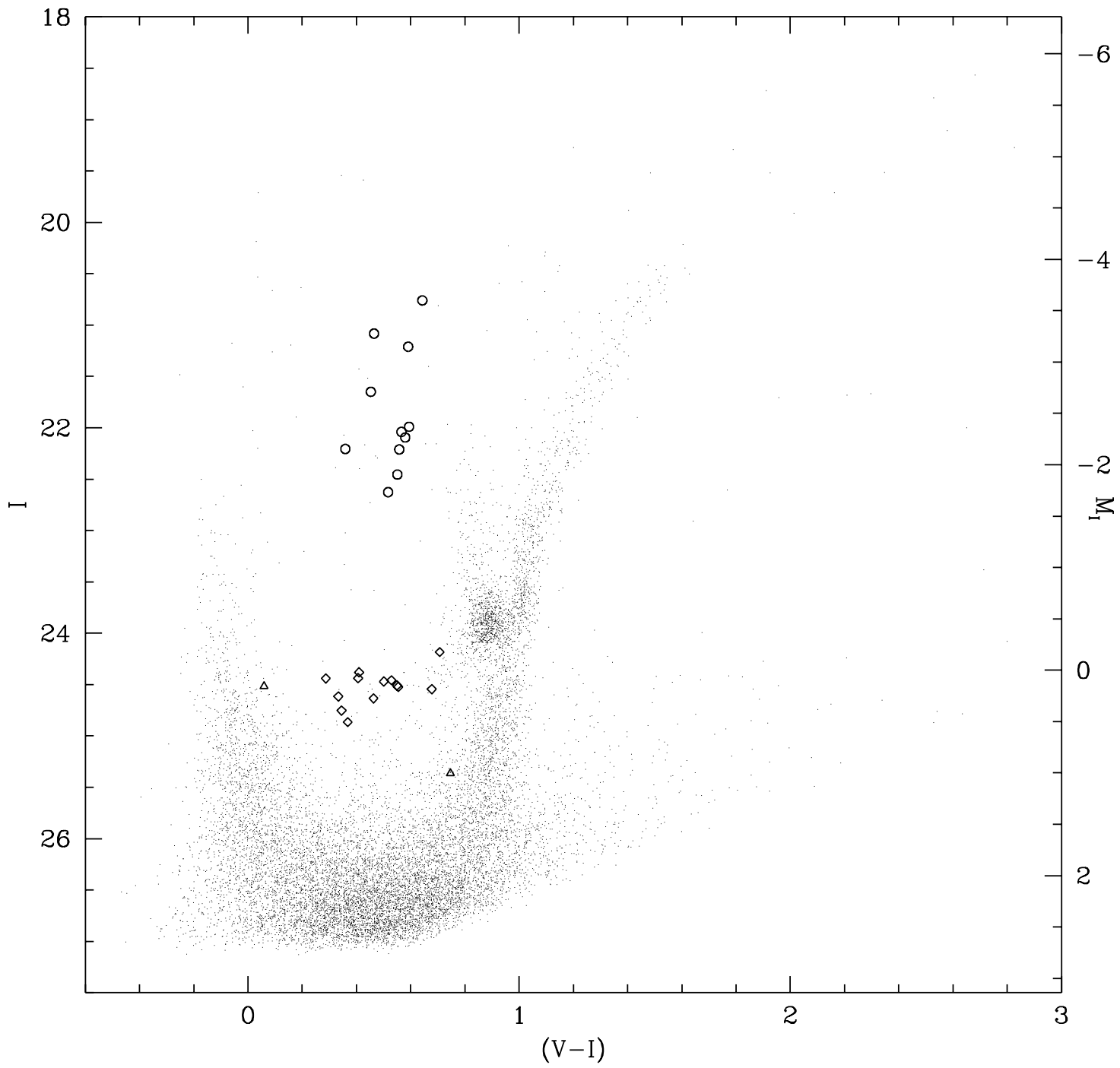
18
20
22
24
26
I
−6
−4
−2
0
2
M_I
0
1
2
3
(V−I)

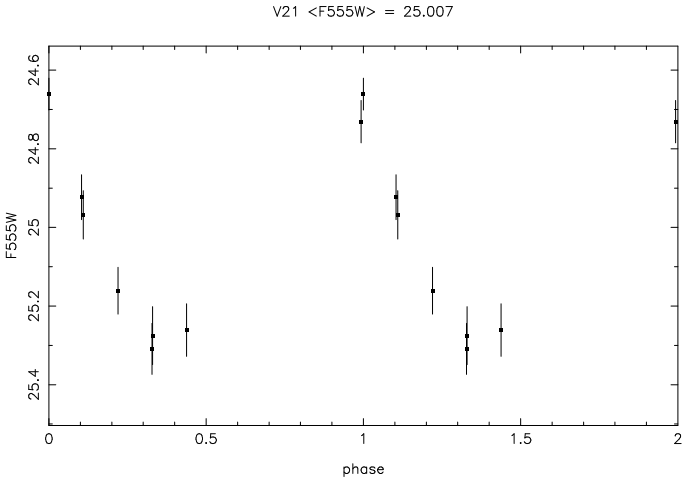
V21 <F555W> = 25.007
F555W
phase

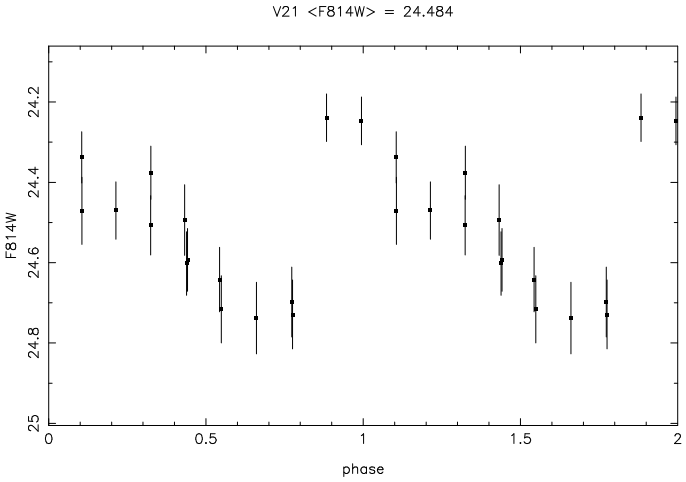
V21 <F814W> = 24.484
F814W
phase

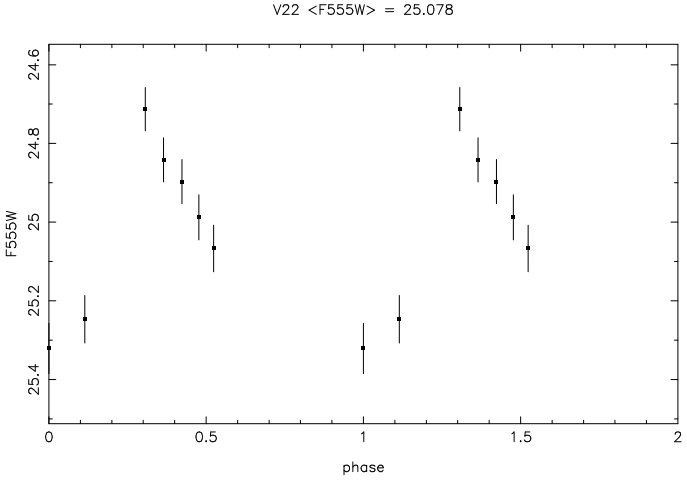
V22 <F555W> = 25.078
F555W
phase

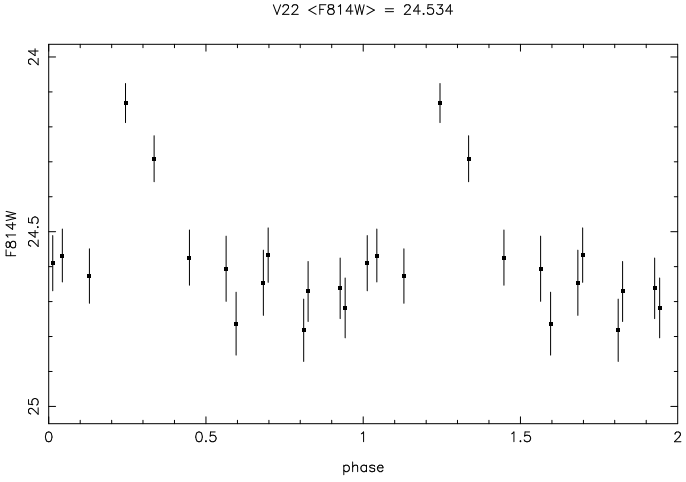
V22 <F814W> = 24.534
F814W
phase

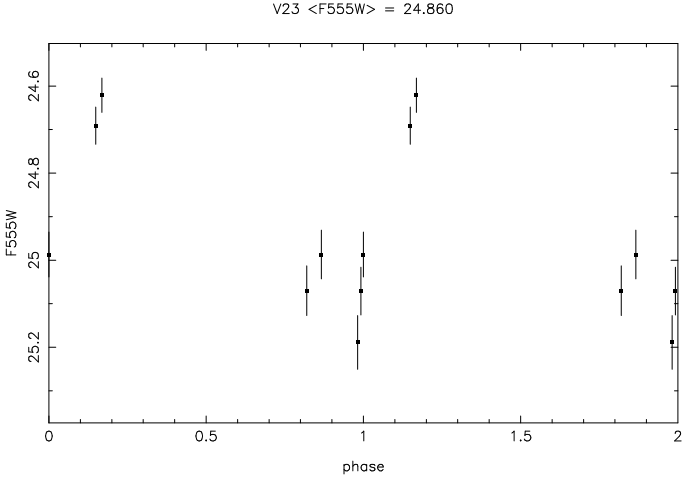
V23 <F555W> = 24.860
F555W
phase

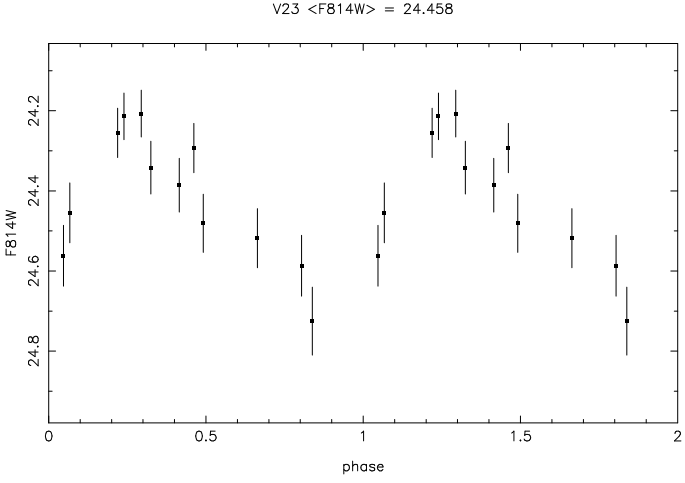
V23 <F814W> = 24.458
F814W
phase

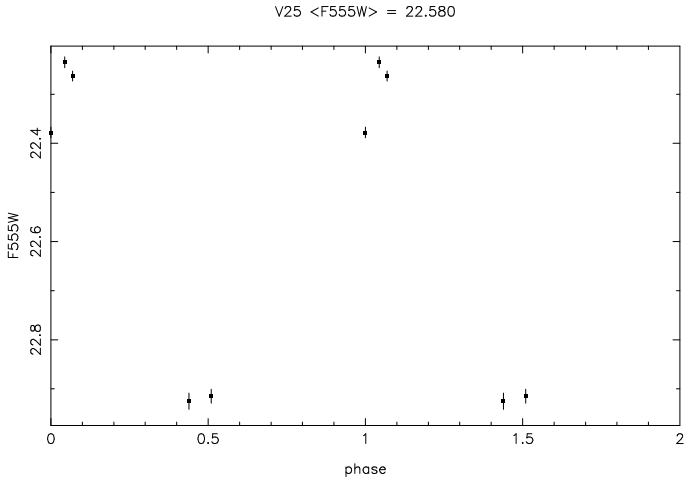
V25 <F555W> = 22.580
F555W
22.4
22.6
22.8
0
0.5
1
1.5
2
phase

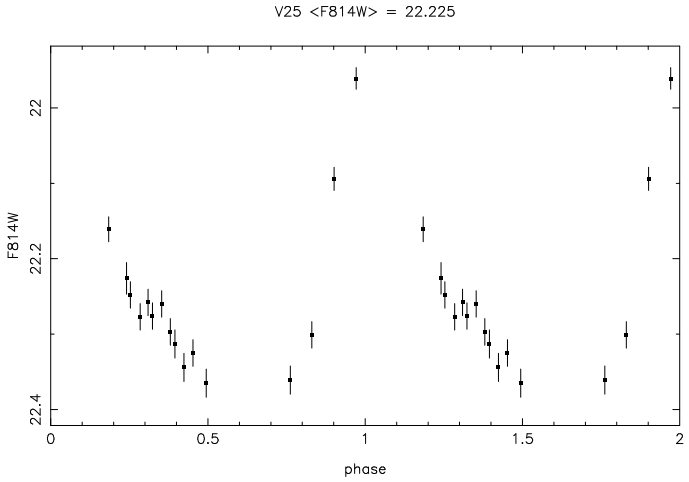
V25 <F814W> = 22.225
F814W
22
22.2
22.4
0
0.5
1
1.5
2
phase

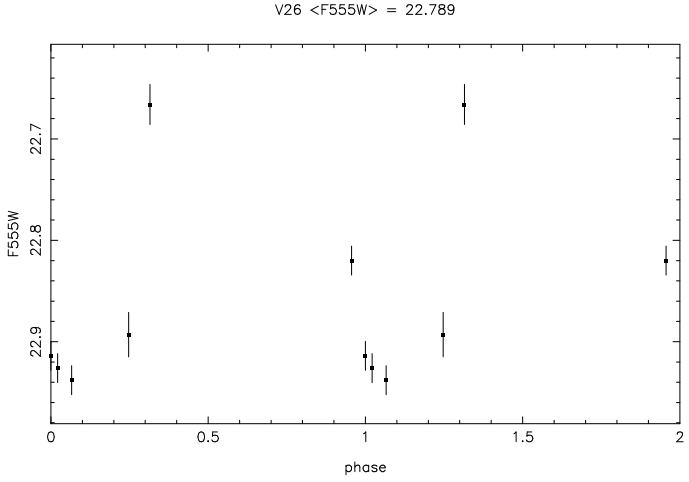
V26 <F555W> = 22.789
F555W
22.7
22.8
22.9
0
0.5
1
1.5
2
phase

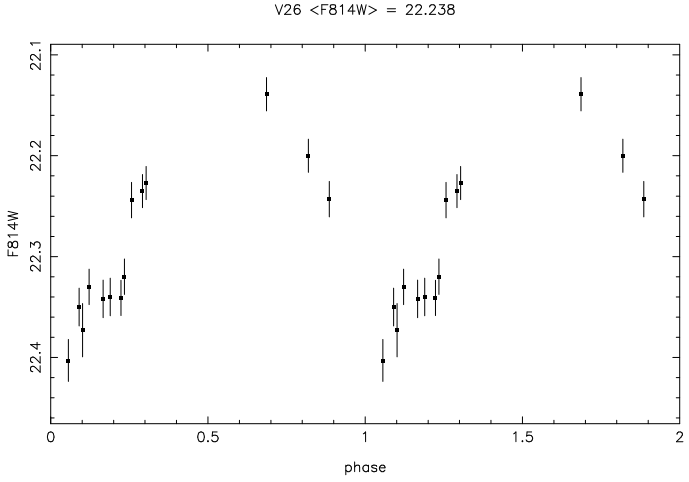
V26 <F814W> = 22.238
F814W
22.1
22.2
22.3
22.4
0
0.5
1
1.5
2
phase

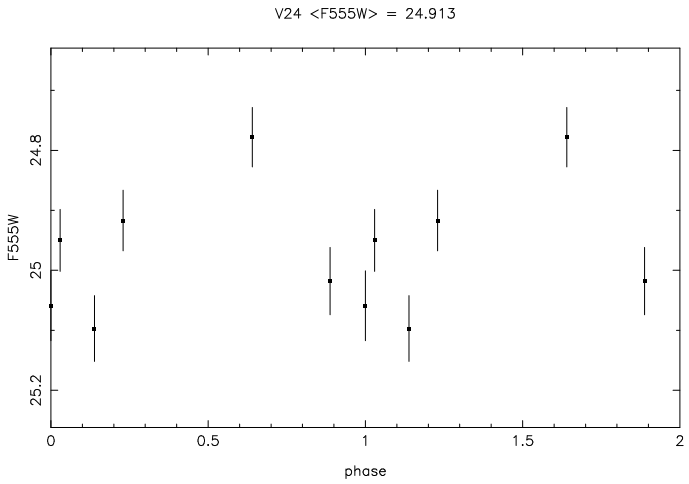
V24 <F555W> = 24.913
F555W
24.8
25
25.2
0
0.5
1
1.5
2
phase

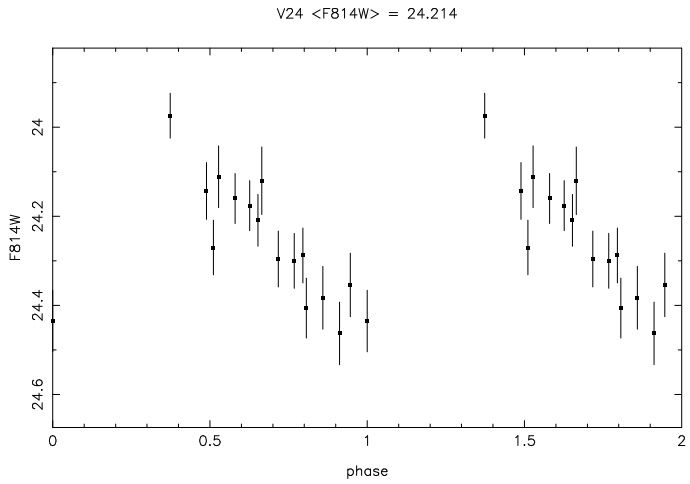
V24 <F814W> = 24.214
F814W
24
24.2
24.4
24.6
0
0.5
1
1.5
2
phase

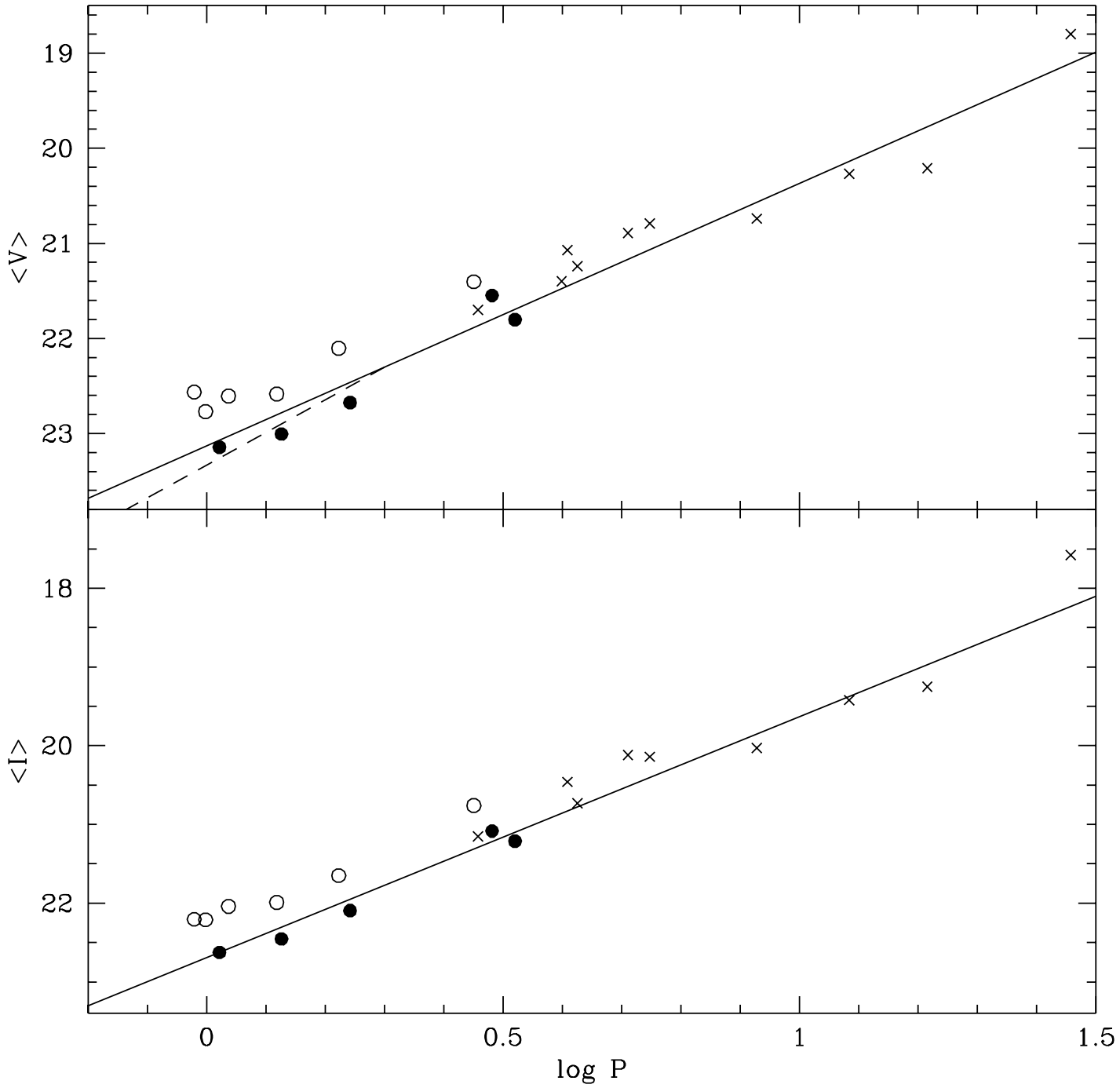
19
20
21
22
23
<V>
18
20
22
<I>
0
0.5
1
1.5
log P

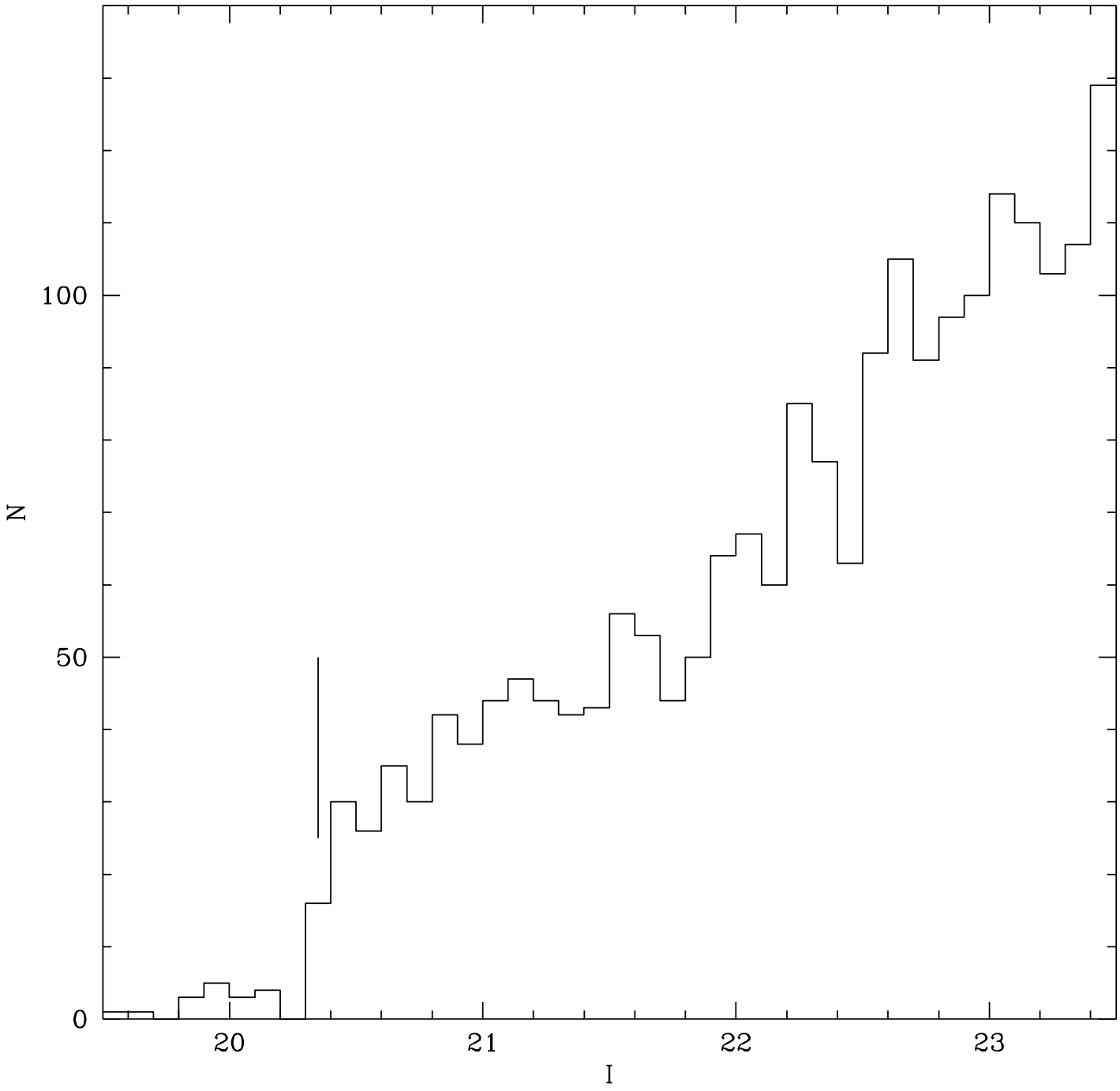
100
50
0
N
20
21
22
23
I

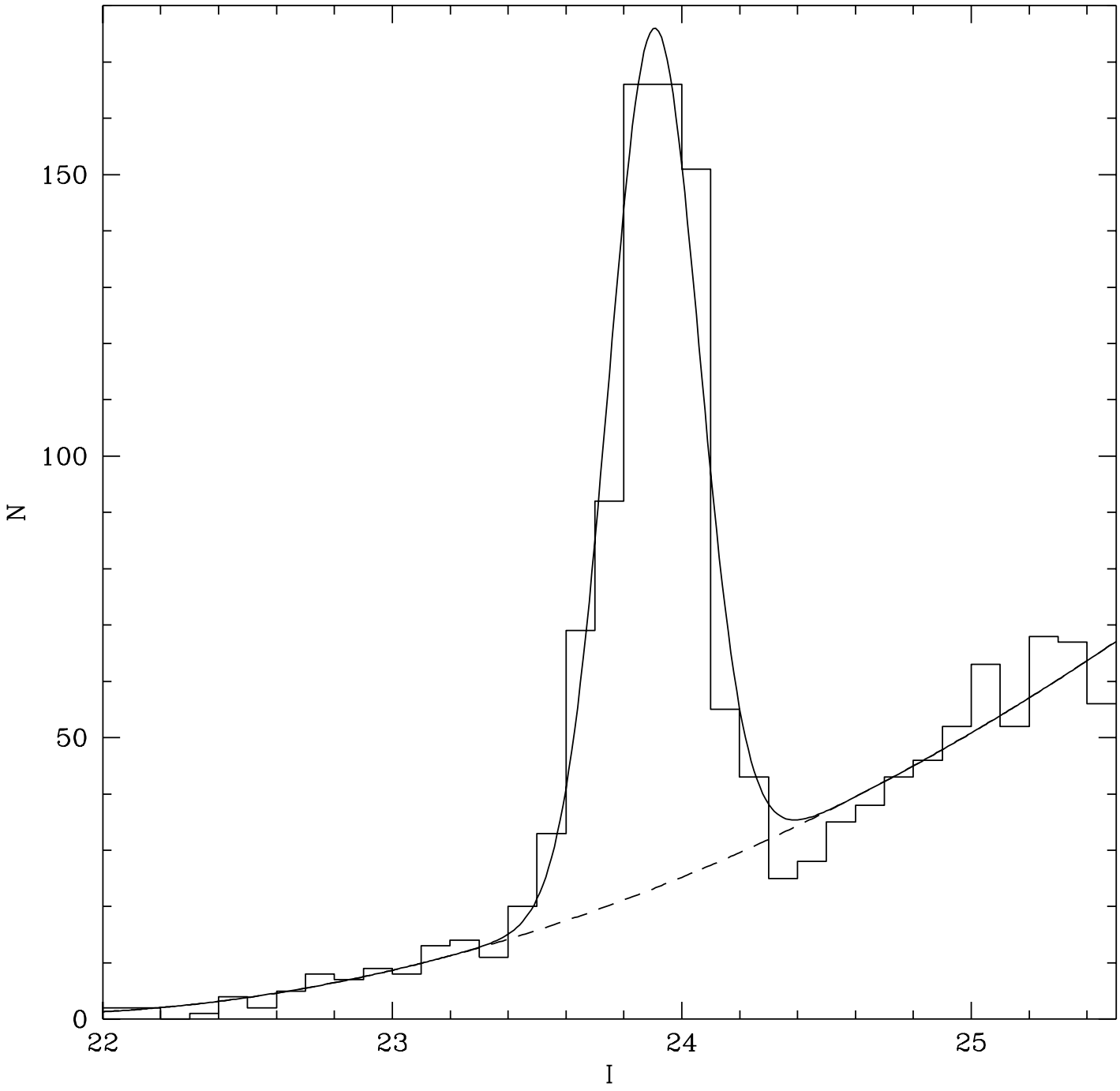
150
100
50
0
N
22
23
24
25
I

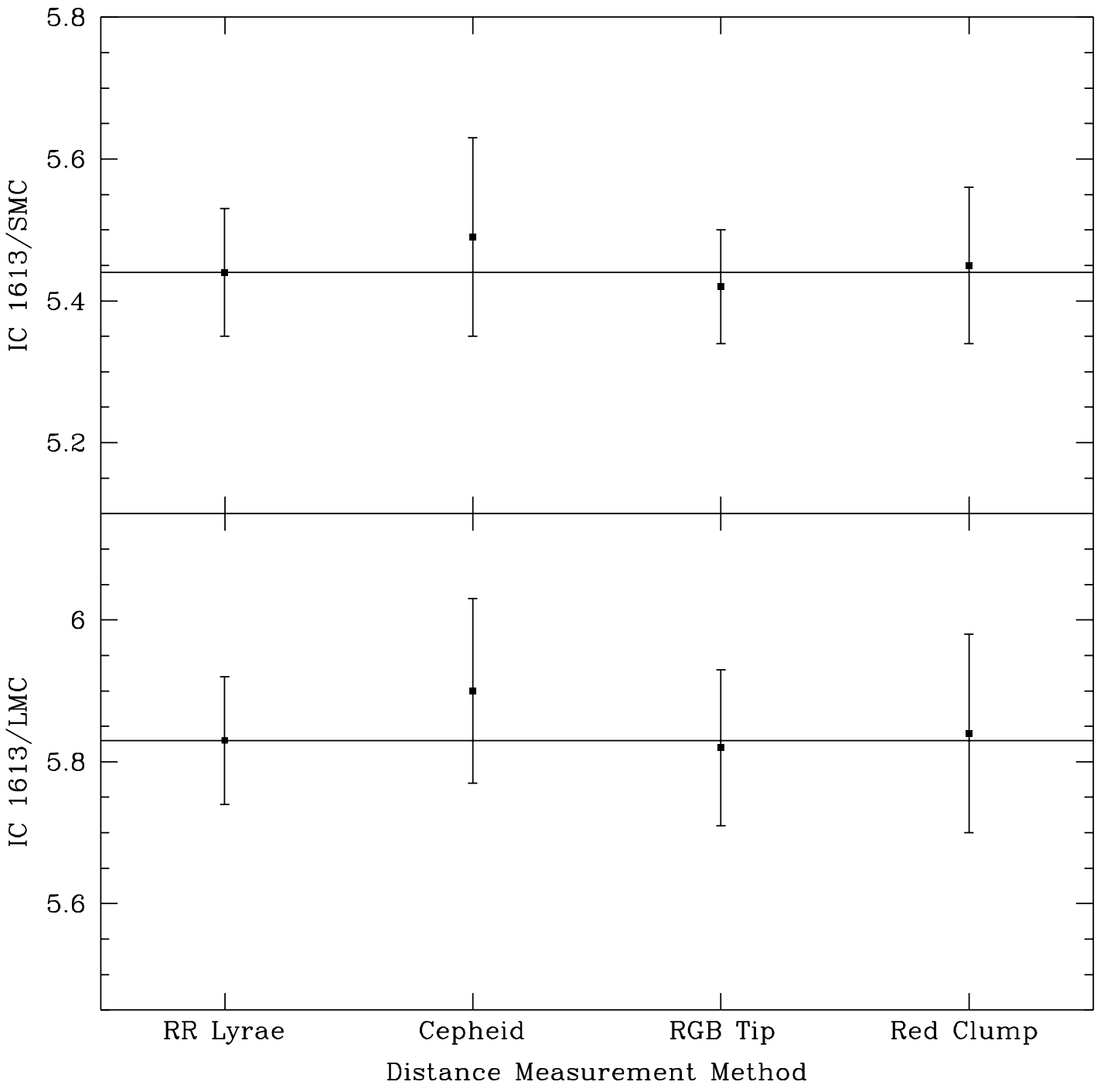
5.8
5.6
5.4
5.2
IC 1613/SMC
6
5.8
5.6
IC 1613/LMC
RR Lyrae
Cepheid
RGB Tip
Red Clump
Distance Measurement Method